WATER RESOURCES RESEARCH, VOL. 49, 2872–2895, doi:10.1002/wrcr.20259, 2013

Modeling the ecohydrological role of aspect-controlled radiation on tree-grass-shrub coexistence in a semiarid climate

Xiaochi Zhou,[1,2] Erkan Istanbulluoglu,[1] and Enrique R. Vivoni[3,4]

Received 22 August 2012; revised 15 April 2013; accepted 15 April 2013; published 28 May 2013.

[1] In this study, an ecohydrological Cellular Automata Tree-Grass-Shrub Simulator (CATGraSS) is presented. CATGraSS is driven by pulses of rainfall and daily solar radiation. In the model, each cell can hold a single plant type (tree, shrub, tree seedlings, shrub seedlings, grass) or can be bare soil. Plant competition is modeled explicitly by keeping track of mortality and establishment of plants, both calculated probabilistically based on soil moisture stress. Topographic influence on incoming shortwave radiation is treated explicitly, which leads to spatial variations in potential evapotranspiration and soil moisture over storm and interstorm time scales, and plant distribution over annual time scales. The model is implemented in a small basin (3.3 km^2) in central New Mexico, USA, where north facing slopes are characterized by a juniper pine and grass savanna, and south facing slopes by creosotebush shrubs and grasses. Representing the current climate by a seasonal-varying Poisson rectangular pulse rainfall model, CATGraSS is calibrated against the existing plant patterns in the study catchment. The model is then used in a series of numerical experiments. CATGraSS is first run on flat terrain to examine the role of topography on plant patterns. Consistent with our observation in the region, this "flat run" gave a shrubland ecosystem with scattered grasses and trees. Model sensitivity to rainfall is investigated in a limited number of simulations by altering rainfall frequency-magnitude statistics, and seasonality. The sensitivity runs suggest that changes in the storm characteristics could lead to a dramatic reorganization of the plant composition on topography in central New Mexico. CATGraSS results underscore the importance of solar irradiance in determining vegetation composition over complex terrain under a water-limited ecosystem.

Citation: Zhou, X. E. Istanbulluoglu, and E. R. Vivoni (2013), Modeling the ecohydrological role of aspect-controlled radiation on tree-grass-shrub coexistence in a semiarid climate, *Water Resour. Res.*, *49*, 2872–2895, doi:10.1002/wrcr.20259.

1. Introduction

[2] Patterns of vegetation on the landscape are mainly a function of the availability of light [*Ricard and Messier*, 1996; *Martens et al*., 2000], nutrients [*Tilman*, 1987; *Lejeune et al*., 2002; *Rietkerk et al*., 2004], and soil moisture [*Klausmeier*, 1999; *Couteron and Lejeune*, 2001] that support plant growth; and other environmental conditions, such as temperature and snow, that determine the timing and length of the growing season [*Myneni et al*., 1997; *Dunne et al*., 2003]. Therefore, plant types and patterns on the landscape are chiefly controlled by climate at the regional scale, and soil texture and topography at the local scale [*Larcher*, 1995; *Svoray and Karnieli*, 2010].

[3] Savannas, where trees and grasses coexist, are responsible for about 26% of the terrestrial gross primary production (GPP) globally [*Beer et al*., 2010]. It has been widely accepted that the structure of savannas is determined by the interactions between climate, resource competition, herbivory, and fire [*Scholes and Archer*, 1997; *Jeltsch et al*., 2000; *Sankaran et al*., 2004]. Two classes of savanna dynamics models have been proposed: (1) competition-based models (CBMs) [e.g., *Walter*, 1971, *Walker et al*., 1981; *Walker and Noy-Meir*, 1982] and (2) demographic-bottleneck models (DBMs) [e.g., *Hochberg et al*., 1994; *Jeltsch et al*., 1996, 1998; *Higgins et al*., 2000; *Accatino et al*., 2010], which have been used to explore savanna dynamics and stability in absence of pronounced topography. Despite the fundamental role of topography on water and energy distribution, little is known how topography controls the dynamics of plant coexistence and patterns in different climates [*Caylor et al*., 2005; *Ivanov et al*., 2008b].

[4] In principle, CBMs are mainly built upon spatial and/or temporal niche separation concepts [*Scholes and*

[1]Department of Civil and Environmental Engineering, University of Washington, Seattle, Washington, USA.
[2]Department of Civil and Environmental Engineering, Duke University, Durham, North Carolina, USA.
[3]School of Earth and Space Exploration, Arizona State University, Tempe, Arizona, USA.
[4]School of Sustainable Engineering and the Built Environment, Arizona State University, Tempe, Arizona, USA.

Corresponding author: E. Istanbulluoglu, Department of Civil and Environmental Engineering, University of Washington, 164 Wilcox Hall, Seattle, WA 98195, USA. (erkani@uw.edu)

0043-1397/13/10.1002/wrcr.20259

Archer, 1997; *Sankaran et al*., 2004] or predator-prey interactions [*Cox*, 2001; *Arora and Boer*, 2006]. The basis of root niche separation (i.e., Walter hypothesis) is a conceptualized two-layer soil moisture model, where grasses with short roots are limited to and superior at exploiting top layer soil moisture, while trees with longer roots have access to both layers [*Walter*, 1971; *Walker et al*., 1981; *Walker and Noy-Meir*, 1982; *Eagleson and Segarra*, 1985]. The phenological niche separation mechanism elaborates the phenological advantages of trees over grasses [*Scholes and Archer*, 1997; *House et al*., 2003; *Sankaran et al*., 2004]. For example, the longer growing season of deciduous C_3 trees than C_4 grasses give them the opportunity to access resources during both early and late stages of the growing season [*Rutherford and Panagos*, 1982; *Scholes and Archer*, 1997]. Besides the niche separation mechanisms, spatially "lumped" plant competition has also been simulated using predator-prey models, typically based on coupled, first-order, nonlinear differential equations (Lotka-Volterra, L-V, equations) that track the areal coverage of coexisting plants in a region. Such empirical-based models are typically driven by the mortality and colonization rates of species [*Tilman*, 1994], which may be related to soil water stress and therefore climate [*Fernandez-Illescas and Rodriguez-Iturbe*, 2004; *Arora and Boer*, 2006].

[5] The second class of models developed for studying savanna dynamics are the DBMs. In general, DBMs are based on the hypothesis that the stability of savanna ecosystem is maintained by the variability of climate and disturbances such as fire and grazing [*Scholes and Archer*, 1997; *Sankaran et al*., 2004]. In most DBMs, ecosystem dynamics have been described either implicitly by using the modified L-V equations [*Baudena et al*., 2010; *Accatino et al*., 2010] or explicitly by using the cellular automata (CA) models. CA models describe the dynamics of local (lateral) plant interactions by mathematical rules over a domain of regular grids. More broadly, the CA modeling idea allows the integration of niche separation and demographic bottleneck concepts to examine the spatiotemporal dynamics of plant organization and the resulting vegetation patterns and clusters [*Higgins et al*., 2000; *van Wijk and Rodriguez-Iturbe*, 2002; *Scanlon et al*., 2007].

[6] Most CA model applications have emphasized biological processes including seed production, dispersal, and stem growth [*Hochberg et al*., 1994; *Jeltsch et al*., 1996, 1998; *Higgins et al*., 2000]. *Hochberg et al*. [1994] first used a CA model to study the effect of fire and seed dispersal on spatial dynamics of tree species in a humid savanna. *Jeltsch et al*. [1996, 1998] found that the spatial processes and small-scale heterogeneities (e.g., locally increased tree seed density and soil moisture content) are important for tree-grass coexistence in semiarid savannas. The model developed by *Higgins et al*. [2000] suggested that the impact of variations of climate and fire regime on the life history of trees (from seedling to mature) promotes tree-grass coexistence in savannas. Some recent ecohydrological CA models have linked plant competition to plant water stress, driven by intermittent rainfall pulses [*van Wijk and Rodriguez-Iturbe*, 2002; *Fernandez-Illescas and Rodriguez-Iturbe*, 2004], leading to a relationship between the statistical properties of vegetation cluster sizes and interannual rainfall variability. These CA modeling studies underscore the importance of plant interactions with the surrounding environment in maintaining savanna structures [*Jeltsch et al*., 1996; *Rodriguez-Iturbe et al*., 1999] and advocate the concept that local-scale interactions can drive large-scale vegetation patterns [*Scanlon et al*., 2007; *Wooten*, 2001].

[7] Topography mediates patterns of soil moisture and plant productivity and could lead to plant coexistence in certain hillslope aspects and morphologies [e.g., *Ayyad and Dix*, 1964; *Svoray and Karnieli*, 2010; *Forzieri et al*., 2011; *Hwang et al*., 2011]. The savanna models reviewed above take a "flat-earth" approach with a spatially uniform forcing of transpiration. Recently, the role of topography on solar radiation distribution and lateral water flow have been introduced to some ecohydrology models [*Kim and Eltahir*, 2004; *Caylor et al*., 2005; *Ivanov et al*., 2008a, 2008b]. However, these models do not explicitly represent transitional plant dynamics and life histories (e.g., seed dispersal, plant establishment, role of age), which critically dictate plant response to climate change and disturbances. As a result, there is a growing need to develop spatially explicit transitional ecohydrologic CA models to predict: (1) the role of spatially varying resources such as soil moisture and nutrients on vegetation responses, (2) shifts in ecosystem boundaries due to climate change and anthropogenic disturbances over complex terrain (i.e., woody plant encroachment in the southwest United States), and (3) spatially varying geomorphic response and critical zone processes that are tightly coupled with vegetation dynamics.

[8] In this study, we present a spatially explicit Cellular Automata Tree-Grass-Shrub Simulator (CATGraSS). In this model, solar radiation is spatially distributed on topography, leading to spatial variations in evapotranspiration, soil moisture, and plant water stress on the landscape. Plant growth is driven by evapotranspiration, and both plant establishment and mortality are linked to plant water stress. CATGraSS is implemented in a semiarid basin within the Sevilleta National Wildlife Refuge (SNWR), New Mexico (USA), where plant distribution is strongly controlled by topographic aspect, with mesic one-seed juniper (*Juniperus monosperma*) and dense black grama (*Bouteloua eriopoda*) coexisting in the north facing slopes, and xeric creosotebush (*Larrea tridentata*) dominating the south facing slopes.

2. Model Description

[9] CATGraSS uses gridded digital elevation models (DEMs), where each grid cell can be occupied by a single plant functional types (PFT) such as tree, shrub, tree seedlings, shrub seedlings, and grass; or can be empty (bare soil). The model combines the functionality of a simplified dynamic global vegetation model (DGVM), which includes the dynamics of local water balance, plant life, and plant mortality [e.g., *Kucharik et al*., 2000; *Sitch et al*., 2003], with a rule-based probabilistic CA component that simulates seed dispersal and plant establishment processes [e.g., *Jeltsch et al*., 1996, 1998; *van Wijk and Rodriguez-Iturbe*, 2002]. The salient aspect of CATGraSS over other CA models is the spatially explicit treatment of solar radiation on the landscape (Figure 1). CATGraSS is driven by daily

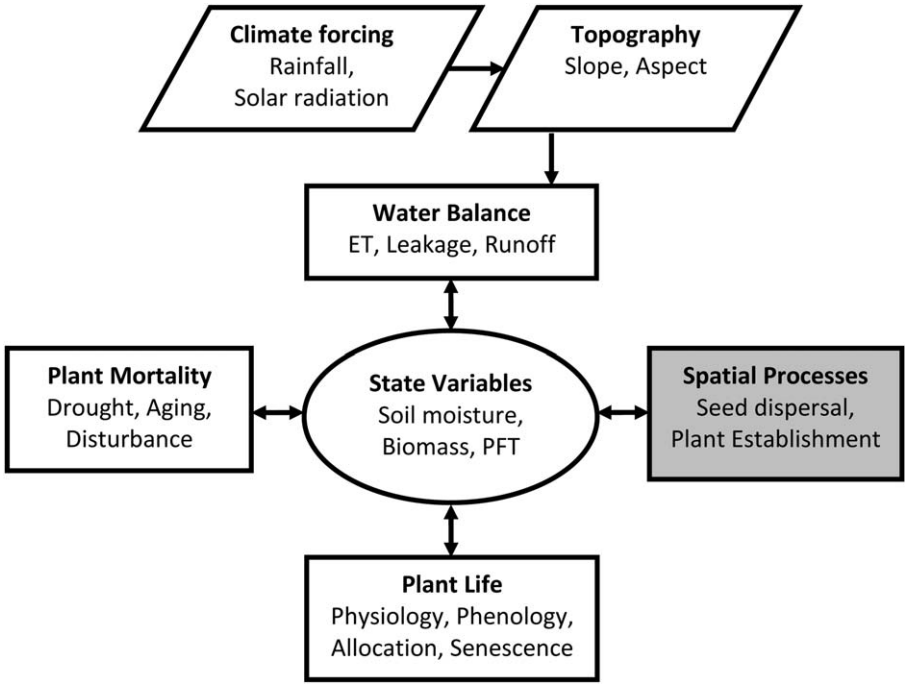

Figure 1. CATGraSS flowchart illustrating the ecohydrological processes (outer rectangles) linked to model state variables in the middle. Components for local (grid cell) processes are represented by boxes with white background and spatially interactive processes are included in box with gray background. PFT, plant functional type.

rainfall and maximum (unstressed) evapotranspiration, ET_{max}. The amount of net radiation used to calculate ET_{max} is estimated as a function of day of year (DOY), slope, and aspect for each PFT.

[10] At each grid cell, CATGraSS tracks the properties of three major local state variables: the root-zone average soil moisture, PFT and its age, and live and dead plant biomass both above and below ground. These state variables are used and updated by local ecohydrological processes that include the root-zone water balance, evapotranspiration (ET), net primary productivity (NPP) driven by ET, NPP allocation to aboveground and belowground biomass pools, plant senescence and mortality, and the spatial processes such as seed dispersal and subsequent plant establishment (Figure 1).

[11] The model can be forced by either observed or generated weather data (the latter for long-term simulations) and can run at either daily or interstorm time steps (driven by instantaneous rainfall pulses). The CA component runs at an annual time step and updates the spatial distribution of PFTs at the beginning of each model year.

2.1. Point Water Balance

[12] The dynamics of depth-averaged root zone water balance is represented by the following differential equation [e.g., *Eagleson*, 1982; *Rodriguez-Iturbe*, 2000]:

$$nZ_r \frac{ds}{dt} = I_a - ET_a(s) - D(s), \tag{1}$$

where n is soil porosity, Z_r (mm) is the effective rooting depth, s is relative saturation (volumetric soil moisture content normalized by n), t (d) is time, I_a (mm d^{-1}) is the rate of actual infiltration, ET_a (mm d^{-1}) is the actual rate of evapotranspiration, and D (mm d^{-1}) is the rate of leakage from the root zone.

[13] The actual rate of infiltration is the amount of rainfall that enters the soil when rainfall depth is larger than canopy interception capacity expressed as

$$I_a = \begin{cases} 0, & P < C_I, \\ \min(p, I_c), & 0 \le s < 1, P > C_I, \\ D & s = 1, P > C_I, \end{cases} \tag{2}$$

where I_c (mm d^{-1}) is the infiltration capacity, p (mm d^{-1}) is the mean rate of rainfall ($p=P/T_r$, where T_r (d) is storm duration), P (mm) is rainfall depth, and C_I (mm) is canopy interception capacity. Infiltration rate is typically higher in undercanopy space than intercanopy space in most semiarid ecosystems, and often varies with vegetation types [*Reid et al.*, 1999; *Bhark and Small*, 2003]. We introduce a canopy-to-intercanopy ratio of infiltration capacity, R_{in}, that scales bare soil infiltration capacity, $I_{c\text{-}b}$, to estimate the infiltration capacity of a vegetated area, $I_{c\text{-}v}$ [*Bhark and Small*, 2003]:

$$I_{c\text{-}v} = R_{in} I_{c\text{-}b}. \tag{3}$$

[14] The canopy interception capacity C_I is approximated by

$$C_I = \min(I_{max} V_t, P V_t), \tag{4}$$

where I_{max} (mm) is the full canopy interception and V_t is the fraction of vegetation cover that includes both dry and

live biomass components. For tree and shrub vegetation types, V_t is assumed to be 1. V_t is thus only used for grass model elements and calculated from the total leaf area index, LAI_t (sum of live and dead leaf area), using an exponential function: $V_t = 1-\exp(-0.75LAI_t)$ [e.g., *Lee*, 1992].

[15] In this model, we assume all rain drops fall vertically (P_V, mm), and the actual amount of rainfall (P) intercepted by the ground is estimated with a cosine correction of the slope angle, S (rad), as $P = P_V \cos(S)$ [*Ivanov et al.*, 2008b].

[16] Maximum (unstressed) evapotranspiration rate used for solving the soil moisture balance of a model element covered by a PFT, ET_{max} (mm d^{-1}), is defined similar to the model used by *Brolsma and Bierkens* [2007]:

$$ET_{max} = \begin{cases} T_{max} - C_I & LAI_l = LAI_{max}, \\ \left[T_{max}\dfrac{LAI_l}{LAI_{max}} + E_b\left(1 - \dfrac{LAI_l}{LAI_{max}}\right)\right] - C_I & LAI_l < LAI_{max}, \end{cases} \quad (5)$$

where T_{max} (mm d^{-1}) is plant maximum transpiration rate, which is calculated for each PFT using the Penman-Monteith equation [*Monteith*, 1965] with LAI_{max}. E_b (mm d^{-1}) is maximum soil evaporation rate. LAI_l is the live leaf area index of the canopy, and LAI_{max} is the maximum LAI_l, given as input to the model. When $LAI_l < LAI_{max}$, T_{max} is scaled by the LAI_l to LAI_{max} ratio, which is assumed to represent the fraction of the area transpiring at the maximum rate. The remaining area fraction is assumed to be subject to potential evaporation rate of a bare soil surface (E_b). To reduce data requirements and keep the model simple, E_b is taken as a fraction (f_b) of the maximum grass transpiration rate, $T_{max\text{-}G}$ (e.g., $E_b = f_b\ T_{max\text{-}G}$) [e.g., *Mutziger et al.*, 2005; *Istanbulluoglu et al.*, 2012]. The value of f_b is set to 0.7 after *Istanbulluoglu et al.* [2012]. C_I is assumed to satisfy the initial atmospheric demand for evapotranspiration. For long-term simulations forced by generated rainfall, T_{max} for each plant type is prescribed by a sinusoidal curve, fitted to Penman-Monteith calculated T_{max} from historical daily weather, and scaled by a T_{max} ratio of a hillslope surface, with given slope and aspect to that of a flat surface (see section 3 for details).

[17] With ET_{max} obtained from equation (5), actual evapotranspiration, ET_a (mm d^{-1}), is calculated using a soil moisture limitation approach as

$$ET_a = ET_{max} \cdot \beta(s), \quad (6)$$

where β_s is an evapotranspiration efficiency term based on the depth-averaged soil moisture in the root zone [e.g., *Dyck*, 1983; *Laio et al.*, 2001]:

$$\beta(s) = \begin{cases} 0, & s_h < s \le s_w \\ \dfrac{s - s_w}{s^* - s_w}, & s_w < s \le s^* \\ 1 & s^* < s \end{cases}, \quad (7)$$

where s_h, s_w, and s^* are soil saturation degree at hygroscopic capacity, wilting point, and incipient stomata closure, respectively [*Laio et al.*, 2001]. For bare soil evaporation, s_w is replaced by s_h.

[18] Surface runoff, R (mm d^{-1}), is generated when $p > I_a$, $R = p - I_a$. The rate of leakage from the root zone is approximated by unsaturated hydraulic conductivity when $s > s_{fc}$ (s_{fc}: soil saturation degree at field capacity), assuming unit hydraulic gradient conditions using: $D(s) = K_s s^{(2b+3)}$, where K_s (mm d^{-1}) is saturated hydraulic conductivity and b is water retention parameter [*Campbell*, 1974].

2.2. Local Plant Dynamics

[19] Net primary productivity (NPP, g DM m^{-2} d^{-1}) of each PFT is calculated as the difference between GPP (g DM m^{-2} d^{-1}) and plant autotrophic respiration (R_e, g DM m^{-2} d^{-1}). GPP is linearly related to daily ET_a by an ecosystem water use efficiency parameter (WUE, kg CO_2 kg^{-1} H_2O), ratio of the amount of carbon gained for unit water loss [*Emmerich*, 2003; *Williams and Albertson*, 2004; *Scott et al.*, 2006].

$$NPP = GPP - R_e = ET_a \cdot WUE \cdot \rho_v \cdot w - R_e, \quad (8)$$

where ρ_v (kg m^{-3}) is water density and w (kg DM kg^{-1} CO_2) converts CO_2 to dry matter. Plant autotrophic respiration (R_e) consists of maintenance (R_m) and growth (R_g) respiration rates, $R_e = R_m + R_g$, which are often related to photosynthesis, Rubisco level, and soil, air, and leaf temperatures [*Collatz et al.*, 1992; *Arora*, 2002]. Through studying the daytime and nighttime net ecosystem CO_2 exchange in an African tree-grass savanna, *Williams and Albertson* [2005] found that R_m could take up approximately 29%–47% of daytime GPP. Here we use a coefficient μ representing the ratio of R_m to GPP, $R_m = \mu \cdot GPP$, following *Arora* [2002]. We assumed R_g is approximately 25% of GPP $- R_m$, $R_g = 0.25(GPP - R_m)$ [e.g., *Ryan*, 1991, *Sitch et al.*, 2003]. Adding R_m and R_g, and substituting into R_e in equation (8) gives NPP as

$$NPP = 0.75 \cdot (1 - \mu) \cdot ET_a \cdot WUE \cdot \rho_v \cdot w. \quad (9)$$

[20] In this paper we assumed WUE as a PFT-dependent constant. One way to calculate WUE is based on the Fick's law of diffusion, and relates WUE to the water vapor pressure difference inside the leaf and in the air [*Farquhar et al.*, 1989]. With a constant WUE, the grassland component of this model captured the seasonal variability of grass biomass measured in the field as well as the model with a daily-varying WUE [*Istanbulluoglu et al.*, 2012]. Constant WUE has been used in various other models [e.g., *de Reffye et al.*, 1997; *Yan et al.*, 2004] and supported by some field evidence [e.g., *Grunzweig et al.*, 2003; *Williams and Albertson*, 2004].

[21] The partitioning of NPP is based on the mass balance concept similar to most DGVMs [e.g., *Kucharik et al.*, 2000; *Cramer et al.*, 2001; *Bonan et al.*, 2003; *Sitch et al.*, 2003]. Dynamics of aboveground green/live (B_l), aboveground dead (B_d), and structural (B_s) biomass (g DM m^{-2}) are modeled based on ordinary differential equations [e.g., *Arora*, 2002; *Montaldo et al.*, 2005, 2008; *Williams and Albertson*, 2005; *Ivanov et al.*, 2008a]. B_s consists of both root and sapwood biomass for trees and shrubs, and only represents root biomass for grasses.

$$\frac{dB_l}{dt} = \text{NPP} \cdot \varphi_a - k_{sl}B_l - k_{sf}\xi B_l, \quad (10)$$

$$\frac{dB_s}{dt} = \text{NPP} \cdot (1 - \varphi_a) - k_{ss}B_s, \quad (11)$$

$$\frac{dB_d}{dt} = k_{sl}B_l - k_{dd}\eta_{sd}B_d, \quad (12)$$

where k_{sl} and k_{ss} (d^{-1}) are the senescence (death) coefficients for green/live, and structural biomass, respectively. k_{dd} (d^{-1}) is the decay coefficient for aboveground dead biomass (leaves only, excluding the structural biomass). We did not separate the structural biomass into live and dead components. In the simulation, k_{sl} and k_{ss} are used in both the growing and dormancy periods. During dormancy, k_{sl} is doubled to represent the environmental conditions that enhance the rate of death. NPP is partitioned between B_l and B_s using an allocation coefficient, φ_a, which depends on available space. The allocation coefficient for grass ($\varphi_{a\text{-}G}$) is taken from *Istanbulluoglu et al*. [2012], and those for woody plants ($\varphi_{a\text{-}W}$, e.g., shrubs and trees) are based on *Williams and Albertson* [2005]:

$$\varphi_{a\text{-}G} = 1 - \frac{\text{LAI}_l}{\text{LAI}_{\max} - \text{LAI}_l}, \quad (13)$$

$$\varphi_{a\text{-}W} = 1 - \frac{\text{LAI}_l}{\text{LAI}_{\max}}. \quad (14)$$

[22] In equation (10), k_{sf} (d^{-1}) represents the maximum drought-induced foliage loss rate [*Ivanov et al*., 2008a], and ξ is the mean interstorm water stress defined similar to *Porporato et al*. [2001]:

$$\xi = [1 - \beta(\bar{s})]^M = \begin{cases} 1, & \bar{s} < s_w \\ \left(\dfrac{s^* - \bar{s}}{s^* - s_w}\right)^M, & s_w \le \bar{s} \le s^* \\ 0 & \bar{s} > s^* \end{cases}, \quad (15)$$

where $\bar{s}$ is the mean interstorm soil moisture content and M is a parameter that represents the nonlinear effects of water deficit on plants. We used $M = 4.0$ for all PFTs [*Ivanov et al*., 2008a]. In equation (12), k_{dd} is the rate of maximum decomposition of dead biomass during the peak of the warm season. The adjustment coefficient for dead biomass loss rate η_{sd} is included to introduce the effect of climate, such that the rate of decomposition is at its maximum level when $T_{\max}$ reaches a threshold value using the $T_{\max}/T_{d\text{-max}}$ ratio:

$$\eta_{sd} = \min\left(T_{\max}/T_{d-\max}, 1\right), \quad (16)$$

where $T_{d\text{-max}}$ (mm d^{-1}) is a calibration parameter. Application of equation (16) has greatly improved model performance in grasslands [*Istanbulluoglu et al*., 2012]. The specific leaf area for live (c_l) and dead (c_d) biomass are used to calculate live, dead, and total LAI, respectively, as $\text{LAI}_l = c_l B_l$, $\text{LAI}_d = c_d B_d$, and $\text{LAI}_t = \text{LAI}_l + \text{LAI}_d$.

[23] In DGVMs, the onset and the offset of the growing season is often triggered when a set of environmental conditions (e.g., air and soil temperatures, soil moisture, positive net photosynthesis) are satisfied for a certain period of time [e.g., *Cayrol et al*., 2000; *Sitch et al*., 2003; *Ivanov et al*., 2008a]. In CATGraSS the growing season is only defined for grass vegetation using the 30 day averaged $T_{\max}$, $T_{\text{max-30}}$ (mm d^{-1}), as a surrogate variable for climatic favorability [*Istanbulluoglu et al*., 2012]. The growing season starts when $T_{\text{max-30}}$ is higher than growth threshold (GT), and ends when $T_{\text{max-30}}$ falls below dormancy threshold (DT). This approach is preferred to minimize the model parameters used in long-term simulations.

2.3. CA Component

[24] In CATGraSS, a cell can be occupied by one of the following five plant states: tree, shrub, grass, tree seedling, shrub seedling; or can be unoccupied. Only mature tree and shrubs plants can disperse seeds. Plant establishment only occurs on empty (bare soil) cells and follows a set of rules based on the water stress of neighboring mature plants. After establishing in an unoccupied site, seedlings either continue to grow up to mature plants or die before they mature.

2.3.1. Plant Establishment

[25] The probabilistic plant establishment algorithm is run once a year at the beginning of the growing season at each bare soil cell. We postulate the probability of establishment (P_E) as an aggregate measure of seedling availability from the plant community neighboring the bare soil cell, conditioned on their water stress, and the role of allelopathic interactions between plants.

[26] For grass plant type, we make the assumption that seeds are available for growth everywhere in the simulation domain. Following the earlier CA models of savanna ecosystems, we assume shrubs provide seeds to their first ring of surrounding neighboring cells (8 cells); and trees provide seeds to their both first and second ring of neighboring cells (16 cells) [*Jeltsch et al*., 1996; *van Wijk and Rodriguez-Iturbe*, 2002]. Tree and shrub seedlings cannot send seeds until they become mature.

[27] Based on the proposed seed dispersal strategy, we postulate that P_E can be related to the ecohydrological "well-being" of the seedling sources (i.e., the neighboring plants). To measure this plant well-being, we introduce a plant live index, ϕ, defined as one minus a normalized cumulative plant water stress, WS. WS is calculated as the sum of the mean interstorm water stress (equation (15)) multiplied by its interstorm duration (T_b, (d)), divided by the growing season length, T_G (d), similar to *Istanbulluoglu and Bras* [2006]:

$$\phi = 1 - \text{WS}, \quad (17a)$$

$$\text{WS} = \frac{\sum^{N_{is}} (\xi \cdot T_b)}{T_G}, \quad (17b)$$

where N_{is} is the number of interstorm events during a growing season.

[28] The plant live index, ϕ, is calculated at the end of each growing season for each model cell in the first ring (I), for mature shrub neighbors (ϕ^I_{SH}), and both first (I) and second (II) rings, for mature tree neighbors (ϕ^I_T and ϕ^{II}_T, respectively), of a bare soil cell. Instead of using the values

for individual cells, we estimate the mean live index of mature shrub neighbors ($\overline{\phi_{\mathrm{SH}}}$) and tree neighbors ($\overline{\phi_T}$), and used them to calculate the probability of establishment for these PFTs in the bare cell as

$$\overline{\phi_{\mathrm{SH}}} = \frac{\sum \phi_{\mathrm{SH}}^{I}}{8}, \tag{18}$$

$$\overline{\phi_T} = \frac{\sum \phi_T^{I}}{8} + \frac{\sum \phi_T^{II}}{16}. \tag{19}$$

[29] Since we assume grass seeds are abundant everywhere in the basin [*Jeltsch et al*., 1996; *van Wijk and Rodriguez-Iturbe*, 2002], the mean live index of grasses ($\overline{\phi_G}$) is taken as the averaged live index of all grass cells within the modeled domain located with similar slope ($\pm 2.5°$) and aspect ($\pm 15°$) as the bare cell.

[30] Allelopathy is a biological process in which one organism limits or supports the well-being of another organism by producing biochemical compounds [*Rizvi and Rizvi*, 1992]. A second component in the calculation of establishment probability relates with the allelopathy phenomenon, which has also been recognized as a biotic mechanism regulating plant communities in arid and semiarid ecosystems [*Went*, 1955; *Knipe and Herbel*, 1966; *Fowler*, 1986; *Escudero et al*., 2000]. *Went* [1955] first attributed the regular spacing of creosotebushes to the toxic substances produced by its roots that can kill other plants. *Knipe and Herbel* [1966] analyzed the germination and growth of semiarid grassland species treated with aqueous extract from creosotebush. Their data indicate that the germination of grasses (e.g., *black grama*) is significantly reduced, while shrub species were not affected.

[31] In the application of CATGraSS in central New Mexico, USA, we assume that creosotebush shrubs only influence grasses based on the work of *Knipe and Herbel* [1966]. Allelopathy is incorporated in CATGraSS by using an inhibitory factor, IN_G, with a subscript G referring to the PFT affected by the allelochemicals produced by shrub, which is limited to grasses in this study. IN_G is defined for each shrub cell. *Knipe and Herbel* [1966] indicated that the inhibition effect increases with the concentration of the extract from creosotebush roots. Therefore, a cumulative inhibition effect is calculated as the product of single shrub inhibition factor on grass (IN_G) and the number of shrub cells in the first ring (N^I) of a bare soil cell, $\mathrm{IN}_G \cdot N^I$.

[32] Finally, the plant establishment probability for grasses ($P_{E\text{-}G}$), tree ($P_{E\text{-}T}$), and shrub ($P_{E\text{-SH}}$) on a bare soil cell are defined as

$$P_{E\text{-}G} = \min\left(\frac{\overline{\phi_G}}{\mathrm{IN}_G \cdot N^I}, P_{E\text{-max-}G}\right), \tag{20a}$$

$$P_{E\text{-SH}} = \min\left(\overline{\phi_{\mathrm{SH}}}, P_{E\text{-max-SH}}\right), \tag{20b}$$

$$P_{E\text{-}T} = \min\left(\overline{\phi_T}, P_{E\text{-max-}T}\right). \tag{20c}$$

[33] A maximal establishment probability value, $P_{E\text{-max}}$ is introduced for all PFTs as an upper limit to prevent unrealistically fast plant colonization rate [*Jeltsch et al*., 1996; *van Wijk and Rodriguez-Iturbe*, 2002].

[34] The CA rules for plant establishment include the following two major steps. In each annual iteration of the algorithm, all bare soil cells are identified and a "candidate" PFT (tree, shrub, or grass) is randomly selected to establish in each of them. Then, P_E is calculated for the selected PFT (equation 20) and compared with a uniformly distributed random number $\sim U(0,1)$. If the generated number is less than P_E, the selected PFT in the first step is placed in the cell; otherwise, the cell is left bare for a year.

2.3.2. Plant Mortality

[35] In the model application, plant mortality removes the plant from a cell and sets the cell status to bare soil, opening the cell for competition for establishment. Plant mortality is also treated probabilistically and operates at the end of the year. Annual probability of plant mortality (P_M) is defined as the sum of three probabilities: drought stress (P_{Md}), plant aging (P_{Ma}), and local disturbance (P_{Mb}) such as grazing and fire:

$$P_M = \min\left(P_{Md} + P_{Ma} + P_{Mb}, 1\right), \tag{21}$$

[36] P_{Md} is calculated as WS, minus a PFT-specific drought resistance threshold value, θ similar to *van Wijk and Rodriguez-Iturbe* [2002]:

$$P_{Md} = \max\left(\mathrm{WS} - \theta, 0\right). \tag{22}$$

[37] Mortality due to aging is caused by the accumulation of physiological changes that are associated with increased susceptibility to diseases and other environmental factors, which finally leads to death with advancing age [*Watkinson*, 1992]. Age-driven mortality is modeled for woody plants (trees and shrubs) following *Jeltsch et al*. [1998]:

$$P_{Ma} = \begin{cases} 0, & t_p \le 0.5t_{p\text{-max}} \\ \dfrac{t_p - 0.5t_{p\text{-max}}}{0.5t_{p\text{-max}}}, & 0.5t_{p\text{-max}} < t_p \le t_{p\text{-max}} \end{cases}, \tag{23}$$

where $t_{p\text{-max}}$ (yr) is the maximum age and t_p (yr) is the current age of the plant. In equation (23), mortality due to aging is assumed to be negligible before plant reaches its half-life ($0.5t_{p\text{-max}}$). As aging continues, mortality probability grows linearly with plant age.

[38] Finally, P_{Mb} is introduced as background probability that could incorporate the influence of disturbances, fires, and diseases. In the implementation of the model, P_M is calculated for each plant group and compared with a random number, $\sim U(0,1)$. A plant is removed when P_M is greater than the generated number.

3. Spatial Patterns in Evapotranspiration

[39] CATGraSS is designed to perform long-term simulations (thousands of years) to examine the development of vegetation patterns. To improve computational efficiency, we classify topography into topographically similar slope and aspect (S-A) groups. In each of the S-A group, the coupled water balance and biomass production equations (equations (1)–(16)) are run for all PFTs separately. In

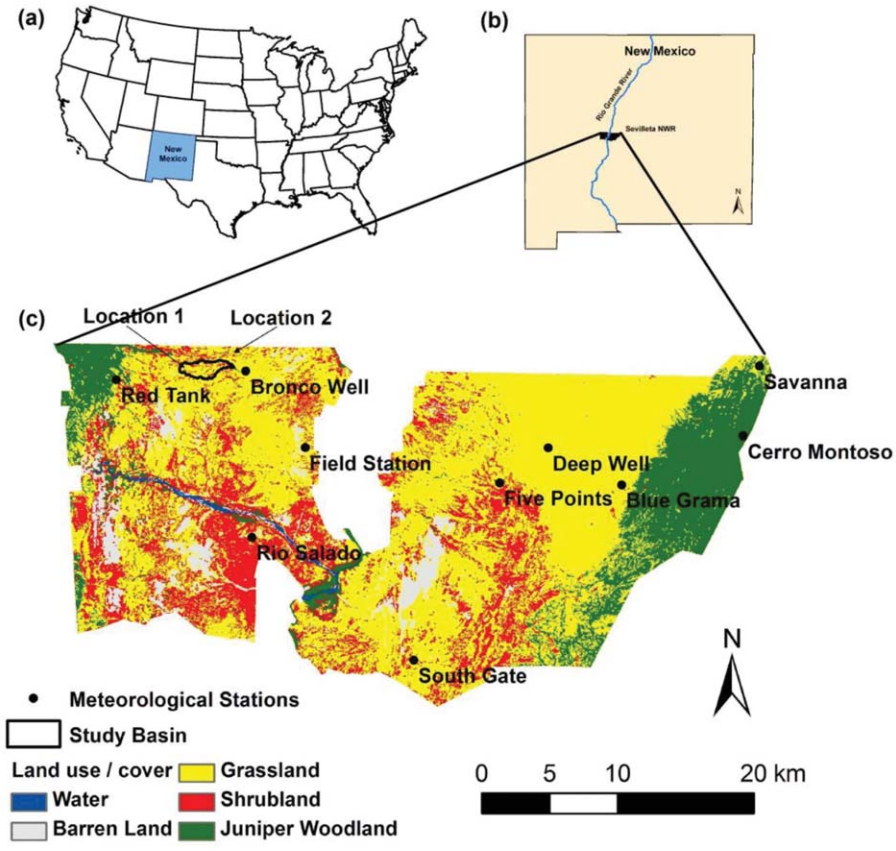

Figure 2. Location of the study site in central New Mexico: (a) The U.S. map, (b) the state of New Mexico map, with the SNWR located along the Rio Grande, and (c) the land use and land cover map of the SNWR, overlain by the watershed boundaries of the study site (northwestern corner). Locations 1 and 2 indicate the points of field photography shown in Figure 3.

our study site in central New Mexico, where the model is implemented, this classification is performed with a 5° increment for slope (0–45°) and a 30° increment for aspect (0–360°), which leads to 118 different S-A groups, including the flat surface. Methods used to calculate $T_{\max}$ for different PFTs in each S-A group are described below.

[40] CATGraSS can be run both by observed and generated weather data. In the case of the former, $T_{\max}$ is estimated by the Penman-Monteith (P-M) equation [e.g., *Shuttleworth*, 1992]. The aerodynamic resistance r_a (s/m) of the P-M equation is calculated following *Allen et al.* [1998] as a function of wind speed, vegetation height, and heights at which wind and relative humidity were measured. The canopy resistance r_s (s/m) of the P-M equation is obtained from the stomatal resistance of a well-illuminated leaf in the absence of any water limitations and other environmental stress factors, r_l (s/m), scaled by the sunlit fraction of $\mathrm{LAI_l}$ (taken half the $\mathrm{LAI_l}$): $r_s = r_l/(0.5\mathrm{LAI}_{\max})$ [e.g., *Allen et al.*, 1998].

[41] The influence of topography is introduced in the calculation of net radiation, R_n (W/m^2), by postulating that the daily incoming shortwave radiation on topographical elements within a S-A group, $R_{s\text{-}H}$ (W/m^2), and on a flat surface, $R_{s\text{-}F}$ (W/m^2) (from observations), can be related through a radiation factor f_R. It is assumed that both hillslope and flat landscape elements have identical cloud cover [e.g., *Dingman*, 2002]:

$$R_{s\text{-}H} = f_R \cdot R_{s\text{-}F}, \tag{24}$$

$$f_R = \frac{R_{c\text{-}H}}{R_{c\text{-}F}}, \tag{25}$$

where $R_{c\text{-}H}$ and $R_{c\text{-}F}$ (W/m^2) are the clear-sky incoming shortwave radiation for a S-A group and a flat surface, respectively ($f_R = 1$ for flat surface). For all S-A groups, the model proposed by *Allen et al.* [2006] is used to calculate $R_{c\text{-}H}$ (including $R_{c\text{-}F}$) as a function of the DOY, latitude, slope, and aspect angles at the midpoints of the S-A ranges, with the clear-sky atmospheric transmissivity coefficient obtained from *Bras* [1990]. Calculated f_R values for 118 S-A groups for each DOY are compiled into a lookup table and used in the model for all simulations.

[42] The net radiation (R_n) on the terrain for each PFT is calculated based on the approximation of the radiation balance [e.g., *Caylor et al.*, 2005]:

$$R_n = (1-\alpha_s) f_R \cdot R_{s-F} + \sigma T_s^4 - \sigma(T_a + 273.15)^4, \tag{26}$$

where α_s is the shortwave albedo. σ is the Stefan-Boltzmann constant (5.67×10^{-8} W m^{-2} K^{-4}). T_a (°C) is the air

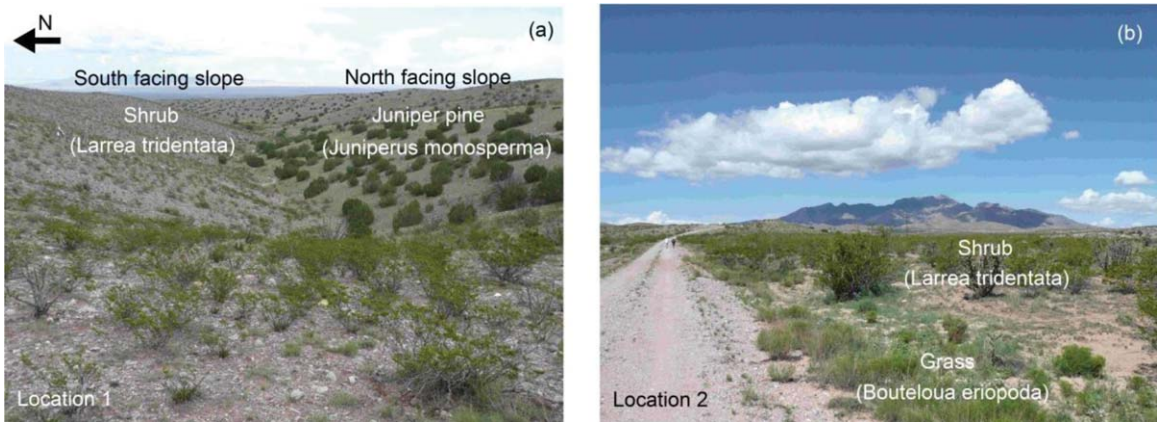

Figure 3. Distribution of PFTs in relation to topography: (a) photograph taken at Location 1 looking eastward from the headwater of the study basin. South facing (north facing) slopes are covered by shrub (tree-grass savanna) and (b) photograph taken at Location 2, looking in the northwest direction. Dominant vegetation is shrub. Scattered trees and limited grass clumps also exist.

temperature used to estimate the outgoing longwave radiation, assuming that vegetation surface and air temperatures are equal. T_s (K) is the apparent radiative temperature of the atmosphere, approximated empirically from *Friend* [1995], used to estimate the incoming longwave radiation in equation (26) as

$$T_s = T_a + 273.15 - 0.825 \cdot \exp\left(3.54 \cdot 10^{-3} f_R \cdot R_{s\text{-}F}\right). \quad (27)$$

[43] Applying equations (24)–(27), $T_{\max}$ can be estimated for all S-A groups ($T_{\max\text{-}H}$) including flat surface ($T_{\max\text{-}F}$) using the P-M method based on historical weather data.

[44] In the case of running long-term simulations with generated storms, CATGraSS is forced by a prescribed $T_{\max}$, which is a sinusoidal function of DOY. This $T_{\max}$ is calibrated to the time series of $T_{\max\text{-}F}$, which is estimated from equations (24)–(27) based on the locally observed weather data [e.g., *Small*, 2005]:

$$T^{\mathrm{Cos}}_{\max\text{-}F} = \frac{\Delta_d}{2}\cos\left[2\pi\left(\frac{\mathrm{DOY} - L_T - N_d/2}{N_d}\right)\right] + \overline{T_{\max\text{-}F}}, \quad (28)$$

where Δ_d (mm/d) is the calibrated difference between the maximum and minimum values of daily $T^{\mathrm{Cos}}_{\max\text{-}F}$ throughout the year. L_T (d) is the lag between the peak $T^{\mathrm{Cos}}_{\max\text{-}F}$ and solar forcing. N_d (d) is the number of days in the year. $\overline{T_{\max\text{-}F}}$ (mm/d) is the mean annual rate of $T_{\max\text{-}F}$. In fitting equation (28) to calculated $T_{\max}$ for each PFT at the central NM study site, L_T assumed to be 0, and Δ_d is calibrated using the method of least squares.

[45] To scale the estimated $T^{\mathrm{Cos}}_{\max\text{-}F}$ from the cosine curve to a given hillslope, we used a transpiration ratio, f_T, defined as the ratio of mean daily $T_{\max}$ of a PFT for a S-A group, $\overline{T}_{\max\text{-}H}$, to that for a flat terrain, $\overline{T}_{\max\text{-}F}$ ($f_T = 1$ for flat surface). $\overline{T}_{\max\text{-}H}$ ($\overline{T}_{\max\text{-}F}$) is obtained by averaging $T_{\max\text{-}H}$ ($T_{\max\text{-}F}$) for a specific DOY over observational years based on a long-term weather data. A lookup table for f_T is compiled for each PFT as a DOY and S-A group matrix (365 by 118). No year-to-year variation in f_T is considered:

$$f_T(\mathrm{DOY}, \text{S-A}, \mathrm{PFT}) = \frac{\overline{T}_{\max\text{-}H}}{\overline{T}_{\max\text{-}F}}, \quad (29)$$

[46] With the f_T lookup table derived above, $T_{\max\text{-}H}$ of a given S-A group is calculated by scaling $T^{\mathrm{Cos}}_{\max\text{-}F}$ with the corresponding f_T ratio of the PFT of interest as

$$T_{\max\text{-}H} = f_T \cdot T^{\mathrm{Cos}}_{\max\text{-}F}. \quad (30)$$

4. Study Site

[47] The CATGraSS is implemented in a catchment in the northwestern corner of the SNWR, Socorro County, New Mexico (Figure 2). This catchment is located in the elevation range of 1600 to 1700 m, flows from west to east, and has a drainage area of 3.3 km^2, with a main channel length of 4.3 km. The mean annual precipitation (MAP) is ~250 mm, composed of a high-intensity summer monsoon season (July to September) during which approximately 50% of the MAP falls, and low-intensity winter rainfalls, controlled by broad-scale frontal systems [*Gosz et al.*, 1995; *Gutiérrez-Jurado et al.*, 2007].

[48] The most profound characteristic of this study basin is the distinct vegetation patterns, with contrasting plant types occupying opposite north (N) and south (S) hillslope aspects (Figure 3a) [*Gutiérrez-Jurado et al.*, 2006]. In the north facing slopes, mesic one-seed juniper (*J. monosperma*) and dense black grama (*B. eriopoda*) coexist. In the south facing slopes, xeric creosotebush (*L. tridentata*) is the dominating plant type, with sparse fluff grass (*Erioneuron pulchellum*) [*McMahon*, 1998]. Juniper pine and creosotebush are evergreen species [*Lajtha and Whitford*, 1989; *Lajtha and Getz*, 1993]. Black grama (C_4 grass) was found to have a strong seasonal phenology [*Kurc and Small*, 2004]. In flat terrain, shrubs dominate with scattered grasses and individual trees in the region (Figure 3b).

[49] The basin is an alluvial fan deposit of the Sierra Ladrones formation [*Green and Jones*, 1997]. Sandy loam texture, overlain by a gravelly desert pavement, generally characterizes the soil type in the basin [*Gutiérrez-Jurado*

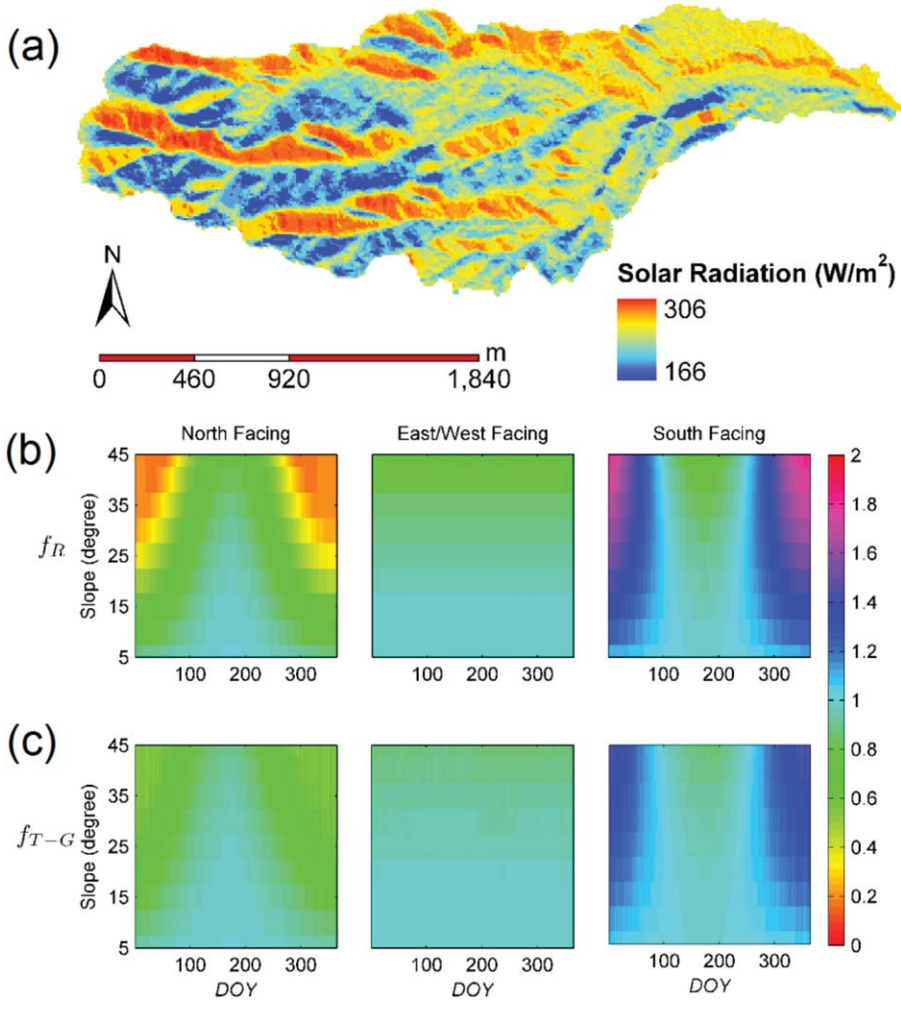

Figure 4. (a) Simulated mean daily incoming clear-sky shortwave radiation over the study area over a year, (b) the clear-sky shortwave radiation ratio (f_R), and (c) transpiration ratio ($f_{T\text{-}G}$) plotted as a function of DOY and terrain slope for four major cardinal directions (east and west reported on the same figure).

et al., 2006]. North facing slopes have deeper soils, higher organic matter, $CaCO_3$, and silt and clay contents than south facing slopes [*McMahon*, 1998].

[50] A 10 m Interferometric Synthetic Aperture Radar (IFSAR) DEM is used for the modeling study [*Gesch et al*., 2002]. As characterized from the DEM, the slope angle in the basin ranges from nearly flat surfaces to as high as 41° on hillslopes, with an average of 8.7°. To illustrate the role of topography on incoming solar radiation, the mean daily clear-sky incoming shortwave radiation over the catchment is plotted (Figure 4a). Annually, south facing slopes receive as much as twice the solar radiation received by north facing slopes. Figure 4a also reflects the variation of local topography across the domain, from the more pronounced terrain in the headwaters region with significant differences in irradiance, to moderate hillslopes in the middle of the basin, and finally to a relatively flat valley bottom toward the watershed outlet.

[51] To illustrate the seasonal changes in radiation forcing at the study site (34.2 N, 106.6 E), we plot the clear-sky shortwave radiation ratio, f_R (equation (25)), and the transpiration ratio for grass, $f_{T\text{-}G}$ (equation (30)), for four major aspects as a function of slope and DOY in Figure 4b and 4c, respectively. $f_{T\text{-}G}$ is based on the daily averages of $T_{\max\text{-}G}$ calculated for 19 years of observed weather forcing between 1990 and 2008 at the Deep Well weather station site (see the section 5 for more information about this station and Figure 2c for its location) in different S-A groups and flat terrain calculated by the P-M equation with R_n estimated for each aspect group from equation (26). Plant parameters (r_l, α_s, and $\mathrm{LAI}_{\max}$ for grass) used to generate $f_{T\text{-}G}$ are reported in Table 3. Both f_R and $f_{T\text{-}G}$ show similar patterns with slope and DOY, while the range is smaller for $f_{T\text{-}G}$ due to the role of air temperature and wind speed in the P-M equation.

[52] East (E) and west (W) facing slopes show only a slight decrease in f_R and $f_{T\text{-}G}$ as the terrain slope grows, but no notable response to DOY, indicating that slopes on east and west aspects receive about the same amount of solar radiation as flat terrain. Interestingly, f_R and $f_{T\text{-}G}$ do not show a significant contrast between north and south facing slopes from the beginning of spring until the end of summer (DOY approximately 100–250). In this period, both north and south aspects receive almost identical (on

moderate slopes) and slightly lower (on higher slopes, >25°) solar radiation and maximum transpiration compared to flat terrain surface. Contrasting differences between the north- and south facing slopes can be seen during fall and winter of the northern hemisphere (DOY > 250 and DOY < 100), consistent with *Gutiérrez-Jurado and Vivoni* [2013]. During that period, f_R and $f_{T\text{-}G}$ on south facing slopes are almost always higher than 1 (exposed to more radiation than a flat surface), and grow higher with slope angle. In contrast, f_R and $f_{T\text{-}G}$ on north facing slopes are lower than 1 (exposed to less radiation than flat terrain), and decrease further as slope gets steeper.

5. Results and Discussion

[53] We explore CATGraSS in a series of sensitivity analyses in the study basin. PFTs are defined at a 5 m by 5 m grid cell resolution, approximately the size of a mature juniper pine canopy in northern New Mexico [*Breshears et al*., 1997]. Despite that juniper pines are smaller in our study site (~2–3 m in diameter), a larger cell size is preferred to keep model generality of representing mature juniper pines and to improve computational efficiency. This size is also consistent with the CA modeling study of *van Wijk and Rodriguez-Iturbe* [2002], who used 25 m^2 for the canopy size of a mature tree in a southern Texas savanna. For comparison, the influence of grid size on modeled plant patterns is also illustrated in a simulation that used a 2.5 m by 2.5 m cell size (see section 5.1.3 for details). Grid cells containing PFTs are developed by dividing each 10 m IFSAR DEM grid cell into multiple equal-sized pixels, with identical resolution for all PFTs. Spatial water redistribution is not included in the model, and generated runoff is assumed to exit the basin instantaneously.

[54] Three sets of simulations are performed using CATGraSS:

[55] (1) Base (Calibration) run: CATGraSS is calibrated for the chosen study site to reproduce the observed spatial patterns controlled by hillslope aspect in the region. The local ecohydrological dynamics of the model is tested against soil moisture and evapotranspiration observations at a nearby site.

[56] (2) Flat run: CATGraSS is run at a flat surface by removing the topography within the watershed boundaries and setting the elevations to the basin outlet elevation. This simulation was designed to examine plant patterns in the absence of topography.

[57] (3) Rainfall sensitivity: CATGraSS model sensitivity to rainfall forcing is evaluated by running numerical experiments that involved changes in storm statistics (frequency and magnitude) and rainfall seasonality.

[58] As the initial condition to (1) and (2), PFTs are initialized randomly in space, with identical initial cover fractions in the domain. The output vegetation map of (1) is used as input to all simulations conducted in (3). To maintain the continuity of seed dispersal and avoid boundary effects of the catchment domain, a periodic boundary condition is used. It is assumed that when a mature tree/shrub on or close to the catchment boundary sends seeds to its outside neighbors, an image "seed" will enter through exactly the opposite site of the domain [*van Wijk and Rodriguez-Iturbe*, 2002]. The simulations are run for 10,000 years, forced by statistically generated storms. Daily maximum transpiration is obtained from the cosine function (equation (28)), calibrated to 19 years of calculated $T_{\max\text{-}F}$ for each PFT described below.

[59] CATGraSS can be forced by both observed and statistically generated storm data. In storm generation, we used the Poisson rectangular pulses (PRP) model, with a one-parameter exponential distribution for time between storms (T_b) and storm duration (T_r); and a Gamma distribution for rainfall depth (P_V) conditioned on T_r [e.g., *Eagleson*, 1972; *Ivanov et al*., 2007]. The storm intensity p is calculated as $p = P/T_r$. We considered two rainfall seasons: wet and dry, with seasonal precipitations denoted by P_w and P_d (mm), respectively. The wet season represents the North American Monsoon (NAM) from July to September (3 months), with a total of 50% of the MAP [*Vivoni et al*., 2009].

[60] A weather station with 19 years of hourly weather data (SNWR Deep Well station in Figure 2) is used to obtain rainfall model parameters. It should be mentioned that the Deep Well station is located on a flat grassland around 30 km east of our study site. Two other closest meteorological stations near our study basin (Figure 2) are Red Tank (1766 m above sea level (ASL), MAP = 274 mm) and Bronco Well (1547 m ASL, MAP = 212 mm) [*Moore*, 1989–2008]. Short-term observations in our study catchment record MAP of ~255 mm [*Gutiérrez -Jurado et al*., 2006]. Thus, we choose the Deep Well station, where the site elevation (1600 m ASL) and measured MAP (244 mm) are closer to our study site [*Moore*, 1989–2008].

[61] The PRP rainfall model often fails to accurately represent short-duration and high-intensity storms during typical NAM. To better represent storm characteristics and resulting runoff generation in the study region, storm durations (T_r) are reduced, leading to increased storm intensity (as $p = P/T_r$), which can produce catchment runoff consistent with observations of watersheds of similar or larger sizes in the southwest United States (runoff ratio, 1–3% of MAP) [e.g., *Molnar and Ramirez*, 2001]. Similar to *Collins and Bras* [2010], the T_r is divided by a factor of 4 for both wet and dry seasons, which gives ~0.02 days of mean storm duration in both seasons. To prevent exceptionally high-intensity storms due to this treatment, the lower limit of T_r is taken as 10 min. This procedure generates storms as high as 60 mm/h for a 30 min period in a 200 year experiment. *Gutiérrez -Jurado et al*. [2007] estimated that a ~30 min summer storm of ~50 mm/h observed in the study site had a return period between 150 and 200 years.

Table 1. Parameters of the PRP Model Estimated for the Deep Well Weather Station (1990–2008)[a]

Parameter	Description	Observations
P	MAP (mm)	249.1
P_d	Dry season precipitation (mm)	125.6
P_w	Wet season precipitation (mm)	123.5
T_{bd}	Dry season interstorm period (d)	6.64
T_{bw}	Wet season interstorm period (d)	3.51
T_{rd}	Dry season storm duration (d)	0.084 [0.020]
T_{rw}	Wet season storm duration (d)	0.079 [0.019]
h_d	Mean storm depth dry season (mm)	3.07
h_w	Mean storm depth wet season (mm)	4.79

[a]The reduced values of T_{rd} and T_{rw} are given in brackets.

Table 2. Soil Parameters Used in the Water Balance Component of the Model

Soil Texture	n	s_{fc}	$I_{c\text{-}b}$ (mm/d)	K_s (mm/d)	b
Sandy loam[a]	0.43[b]	0.56[b]	0.83[c]	1.75[d]	4.9[b]

[a]*Soil Survey Staff* [1994].
[b]*Laio et al*., [2001].
[c]*Gutiérrez-Jurado et al*. [2006].
[d]*Bhark and Small* [2003].

The estimated PRP model parameters based on the Deep Well site data are reported in Table 1.

5.1. Base Run

5.1.1. Model Calibration

[62] The purpose of the base run is to calibrate the model against observed vegetation patterns in the field (Figure 3a). As the basis of this calibration, we used a 1 m resolution Light Detection and Ranging (LiDAR)-derived tree vegetation map of the study catchment [*Gutiérrez-Jurado and Vivoni*, 2013]. To develop this map, we first obtained a height map for vegetation and other landscape irregularities by taking the difference between the unfiltered LiDAR field and the filtered (bare-earth) field. Second, a threshold height of 0.75 m, above which a cell is designated as a juniper pine cell, is defined through trial and error by comparing the locations of juniper pines in a recent aerial photo of the basin, with those extracted from the LiDAR map using the selected threshold height.

[63] Soil and vegetation parameters used for simulating local water balance and plant dynamics (e.g., biomass production and loss) are listed in Tables 2–4. The parameters used to model soil water balance, evapotranspiration (ET), and local biomass dynamics (Tables 2 and 3) are largely assigned according to the typical published values employed in ecohydrology and land surface models. We reserved only limited number of parameters for calibration, including plant mortality and establishment parameters (Table 4), and several plant decay coefficients calibrated from the ranges reported in other studies (discussed later). Sources of each parameter are presented as footnotes in Tables 2–4.

[64] The sandy loam soil texture of the field site was identified from the STATSGO database [*Soil Survey Staff*, 1994] and confirmed by field observations [*McMahon*, 1998; *Gutiérrez-Jurado et al*., 2006]. Hydrologic soil parameters (n, s_{fc}, and b) for sandy loam are taken from the values compiled by *Laio et al*. [2001]. The parameters that define the rates of infiltration and leakage ($I_{c\text{-}b}$ and K_s) are obtained from a detailed modeling study at the field site [*Gutiérrez-Jurado et al*., 2006] and observations in the region [*Bhark and Small*, 2003] (Table 2).

[65] Table 3 presents CATGraSS parameters that control local ET and plant biomass dynamics (growth and death). All the parameters, except for four, were directly taken

Table 3. Plant Parameters Used to Simulate Soil Moisture and Vegetation Dynamics

Parameters	Description	Grass	Juniper Pine	Creosotebush
$I_{\max}$	Full canopy interception (mm)	1.0[a]	2.0[a]	1.5[a]
Z_r	Root depth (mm)	300[b]	1300[c]	500[c]
Z_{veg}	Vegetation height (m)	0.3[d]	2.0[c]	1.0[c]
r_l	Stomatal resistance (s/m)	130[d]	270[a]	210[d]
s^*	Saturation degree at stomata closure	0.33[a]	0.22[a]	0.24[a]
s_w	Saturation degree at wilting point	0.13[a]	0.15[a]	0.13[a]
s_h	Saturation degree at soil hygroscopic	0.10[e]	0.10[e]	0.10[e]
$\text{LAI}_{\max}$	Maximum leaf area index (m^2/m^2)	2.0[d]	4.0[c]	2.0[c]
R_{in}	Ratio of canopy-interspace infiltration capacity	1.2[f]	2.0[c]	2.0[g]
WUE	Water use efficiency (kg CO_2 kg^{-1} H_2O)	0.01[h]	0.0045[i]	0.0025[j]
k_{sl}	Senescence (death) coefficient of green/live biomass (d^{-1})	0.012[h]	0.002[k]	0.002[k]
k_{ss}	Senescence (death) coefficient of structural biomass (d^{-1})	0.01[h]	0.005[k]	0.005[k]
k_{dd}	Decay coefficient of aboveground dead biomass (d^{-1})	0.013[h]	0.013[l]	0.013[l]
k_{sf}	Maximum drought induced foliage loss rates (d^{-1})	0.02[m]	0.001[l]	0.02[l]
c_l	Specific leaf area for green/live biomass (m^2 leaf g^{-1} DM)	0.0047[h]	0.004[j]	0.004[f]
c_d	Specific leaf area for dead biomass (m^2 leaf g^{-1} DM)	0.009[h]	0.01[n]	0.01[n]
α_s	Shortwave albedo	0.12[a,l]	0.1[a]	0.15[a]
GT, DT	Growth and dormancy thresholds (mm/d)	3.8, 6.8[h]	N/A[o]	N/A
$T_{d\text{-max}}$	Constant for dead biomass loss adjustment (mm/d)	10[h]	10[hp]	10[hp]

[a]*Caylor et al*., [2005].
[b]*Kurc and Small* [2004].
[c]*Gutiérrez-Jurado et al*., [2006].
[d]*Guan and Wilson* [2009].
[e]*Laio et al*., [2001].
[f]*Bhark and Small* [2003].
[g]*Paul and Litvak* [1964].
[h]*Istanbulluoglu et al*. [2012].
[i]*Lajtha and Getz* [1993].
[j]*Lajtha and Whitford* [1989].
[k]*Montaldo et al*. [2005].
[l]Calibration.
[m]*Ivanov et al*. [2008a].
[n]*Williams and Albertson* [2005].
[o]N/A, not applicable.
[p]Adapted from grass vegetation type.

Table 4. Model Parameters for Modeling Plant Mortality and Establishment

Parameters	Description	Grass	Creosotebush	Creosote Seedling	Juniper Pine	Juniper Seedling
θ	Drought-resistant threshold	0.62	0.80	0.64	0.72	0.57
P_{Mb}	Background mortality probability	0.05	0.01	0.03	0.01	0.03
$P_{E\text{-max}}$	Maximal establishment probability	0.35	0.2	N/A	0.25	N/A
$t_{p\text{-max}}$	Maximum age (yr)	N/A	600[a]	18[b]	350[c]	20[d]

[a]*Bowers et al.* [1995].
[b]*Chew and Chew* [1965].
[c]*Grier et al.* [1992].
[d]*Schott and Pieper* [1986].

from the literature, largely from modeling and field studies conducted in the SNWR, in the southwest United States, or in semiarid ecosystems elsewhere with similar plant types. The decay constants for aboveground dead biomass (k_{dd}) and the maximum drought induced foliage loss (k_{sf}) for juniper pine and creosotebush are identified with calibration. Generally, the calibrated plant parameters in this study are within the ranges reported in the literature for semiarid ecosystems [e.g., *Montaldo et al*., 2005; *Williams and Albertson*, 2005; *Ivanov et al*., 2008a].

[66] Predicted spatial patterns of plants by CATGraSS are most sensitive to the mortality and establishments parameters reported in Table 4 (θ, P_{Mb}, $P_{E\text{-max}}$, $t_{p\text{-max}}$). Besides the maximum age parameter ($t_{p\text{-max}}$) obtained from the literature for juniper pine [*Grier et al*., 1992], juniper pine seedlings [*Schott and Pieper*, 1986], creosotebush [*Bowers et al*., 1995], and creosotebush seedlings [*Chew and Chew*, 1960], the other three parameters (θ, P_{Mb}, $P_{E\text{-max}}$) were calibrated in the model. The conceptual design of the CA component of our model is very similar to that of *van Wijk and Rodriguez-Iturbe* [2002], which was implemented in a semiarid Texas savanna. As such, we adapted the parameters used by *van Wijk and Rodriguez-Iturbe* [2002] as base values, and calibrated through numerous CATGraSS experiments until the predicted plant patterns agreed with the tree cover map derived from LIDAR, and the observed patterns of grass and shrub vegetation types at the study site.

[67] Plant mortality is a key component in the model as it opens space for competition and can set the population density of a plant type in the domain. Therefore, in calibrating the model to the LiDAR-derived tree map, we started with the drought-resistance threshold, θ, used for calculating the probability of drought-induced plant mortality, P_{Md} (equation (22)). In the model, P_{Md} becomes nonzero and grows when water stress exceeds θ. On the global scale, shrubs are more drought resistant than trees and grasses in desert environments [*Zeng et al*., 2008]. *van Wijk and Rodrigues-Iturbe* [2002] suggested a higher drought resistance for trees than grasses in a southern Texas savanna. From high to low drought resistance, we rank the PFTs as creosotebush, juniper pine, and grass, and calibrated θ in the model by keeping this drought-resistance ranking. Plant seedlings are in general more vulnerable to droughts than mature plants [*Fenner*, 1987; *McDowell et al*., 2008], which is also true for both juniper pine and creosotebush [*Johnsen*, 1962; *Chew and Chew*, 1965]. To reflect the higher susceptibility of seedlings to drought, all the seedlings are calibrated to be 20% less drought resistant than mature plants (Table 4).

[68] The background mortality probability (P_{Mb}) represents the influence of local disturbances other than droughts (e.g., fire and diseases) that cause plant death. Due to lack of observations, we use the values for trees and grass reported by *van Wijk and Rodrigues-Iturbe* [2002], with a threefold increased probabilities for tree and shrub seedlings (Table 4).

[69] The allelopathic effect of creosotebush represented in equation (20a) was only considered to act on grasses, following the work of *Knipe and Herbel* [1966], and IN_G is assigned through calibration. During calibration, we first completely neglected the allophetic influence of creosotebush on grass ($\mathrm{IN}_G = 0$). This assumption did not influence the PFT composition for north facing slopes, while the cover fraction of grass significantly increased (>15%) and the cover fraction of creosotebush decreased on south facing slopes. Setting $\mathrm{IN}_G = 2$, which was used in the paper, effectively limited the amount of grasses on south facing slopes, consistent with observations [*McMahon*, 1998].

[70] The maximum probability of establishment parameter, $P_{E\text{-max}}$, has been used in other CA models to define an upper limit for colonization rate of a plant type. Grasses usually have a higher capability for colonization than woody plants [*Jeltsch et al*., 1996; *Zeng et al*., 2008]. To constrain this parameter, we used the value reported for grass ($P_{E\text{-max-}G} = 0.35$) in a Texas savanna by *van Wijk and*

Table 5. Summary of Water Balance for All Rainfall Sensitivity Runs[a]

Simulation Experiment	MAP (mm)	Mean Annual $(R+D)/P$	Mean Annual ET/P	ANPP (g DM m^{-2})
Base run	250	0.043	0.957	66.90
Flat run	250	0.046	0.953	64.40
Increased 20% T_b	250	0.047	0.953	97.79
Decreased 20% T_b	250	0.033	0.967	61.65
Increased P_w	250	0.106	0.893	90.56
No seasonality	250	0.034	0.965	95.62

[a]P_w is wet-season precipitation. MAP is mean annual precipitation. ET, R, D, and P are evapotranspiration, runoff, drainage, and annual precipitation, respectively. Values are averaged over the whole basin after the model reached an equilibrium state (years 5000–10,000).

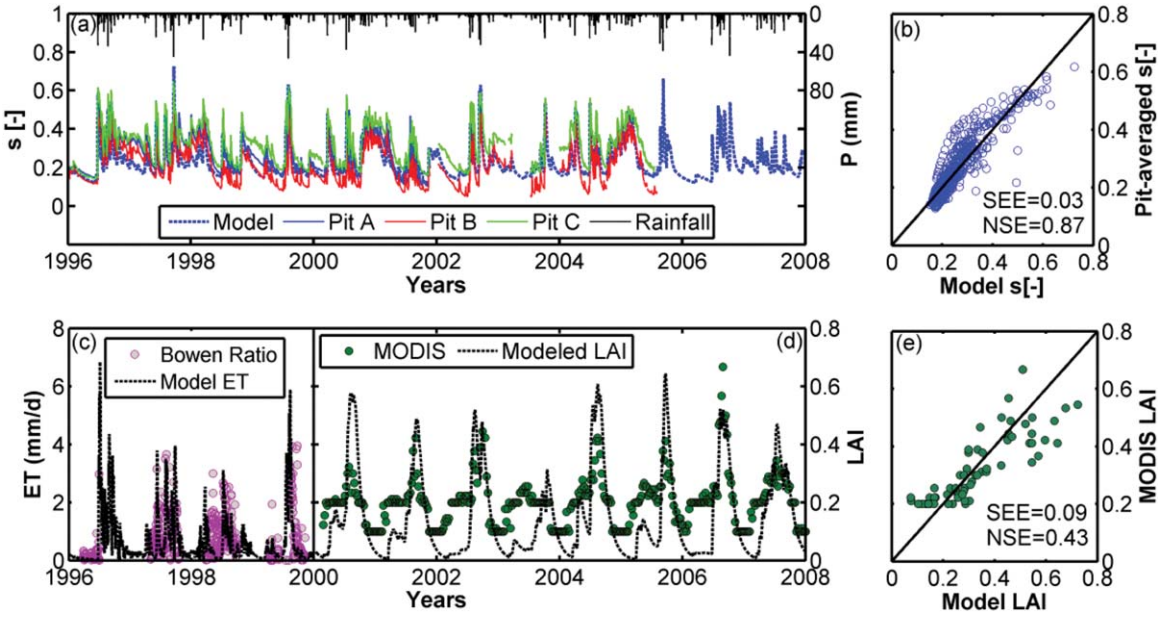

Figure 5. (a) Time series of observed precipitation, and depth-averaged relative soil moisture content (s) in the root zone obtained from model and observations at soil pits; (b) Scatterplot of modeled against pit-averaged s during the growing season; time series of (c) modeled and Bowen ratio-estimated evapotranspiration (ET); (d) modeled and MODIS-derived leaf area index (LAI) for the Deep Well site in the Sevilleta National Wildlife Refuge; and (e) scatterplot of modeled against MODIS-derived LAI for Deep Well site during the growing season.

Rodriguez-Iturbe [2002], and calibrated the value for creosotebush and juniper pine (Table 4). The slightly higher value for juniper pine than creosotebush is consistent with the model of *Zeng et al*. [2008].

[71] To demonstrate the utility of the model in predicting local ecohydrologic dynamics of soil moisture (s), evapotranspiration (ET), and leaf area index (LAI), a limited model confirmation study is performed at the Deep Well meteorological station maintained by the Sevilleta LTER, located on a flat grassland northeast of the SNWR (~30 km east of our study site, Figure 2). The vegetation in the site is mainly C4 grasses, composed of black and blue grama (*B. gracilis*). Deep Well meteorological data includes hourly precipitation, temperature, wind speed, relative humidity, incoming shortwave solar radiation, vapor pressure, soil moisture potential, and soil temperature. The daily averages are calculated for all the weather variables, except for the soil moisture potential and soil temperature, and used in CATGraSS.

[72] Soil moisture is obtained from three different soil pits at 10 and 30 cm depths positioned nearby the Deep Well site, and averaged to represent the daily root-zone-average soil water content. Soil moisture monitoring continues at the site since 1996 using Time Domain Reflectometry (TDR) probes. ET is obtained from an adjacent Bowen ratio tower, which operated from 1996 (only partially) until the end of 1999. The weather variables measured at the Deep Well station, Bowen ratio observations, and soil moisture measurements; and detailed information on their observational design can be found on the Web (J. R. Gosz, Bowen ratio evapotranspiration data, 1996–1999, Sevilleta LTER Database, http://sev.lternet.edu/data/sev-079).

[73] For confirming the modeled live LAI (LAI_l), we used satellite-derived LAI from the Moderate-resolution Imaging Spectroradiometer (MODIS). MODIS data became online in 2000 at a 1 km spatial resolution for every 8 days. The effect of local variability in MODIS LAI is eliminated by taking the mean value of a window of 3 by 3 MODIS grid cells, with the Deep Well site located at the center.

[74] CATGraSS is forced to run at a point using only grass vegetation type from 1996 to the end of 2008. Time series of daily rainfall, and modeled and observed s, ET, and MODIS-derived live LAI are presented in Figure 5. The modeled s shows good agreement with observations at three different pits for the 10 year period between 1996 and 2006, reasonably capturing the timing and magnitude of soil moisture pulses and the slower rate of decays (Figure 5a). To better quantify the ability of CATGraSS in predicting soil moisture dynamics during the growing season, the modeled daily soil moisture is plotted against measured soil moisture (averaged over the three pits) in Figure 5b. The standard error of estimation (SEE) with respect to the one-to-one line and the Nash-Sutcliffe efficiency (NSE) [*Nash and Sutcliffe*, 1970] are reported in Figure 5, showing good agreement between model predictions and field measurements.

[75] The model represents the observed seasonal behavior of ET with some skill (Figure 5c). The model shows a good agreement with observations in 1997, underestimates ET in the first half of 1998, and slightly overestimates ET during the peak of the rainy season in 1999. These discrepancies might result from the highly spatially variable nature of storms in the region, leading to differences in the rainfall received between the rain gage and the footprint of the

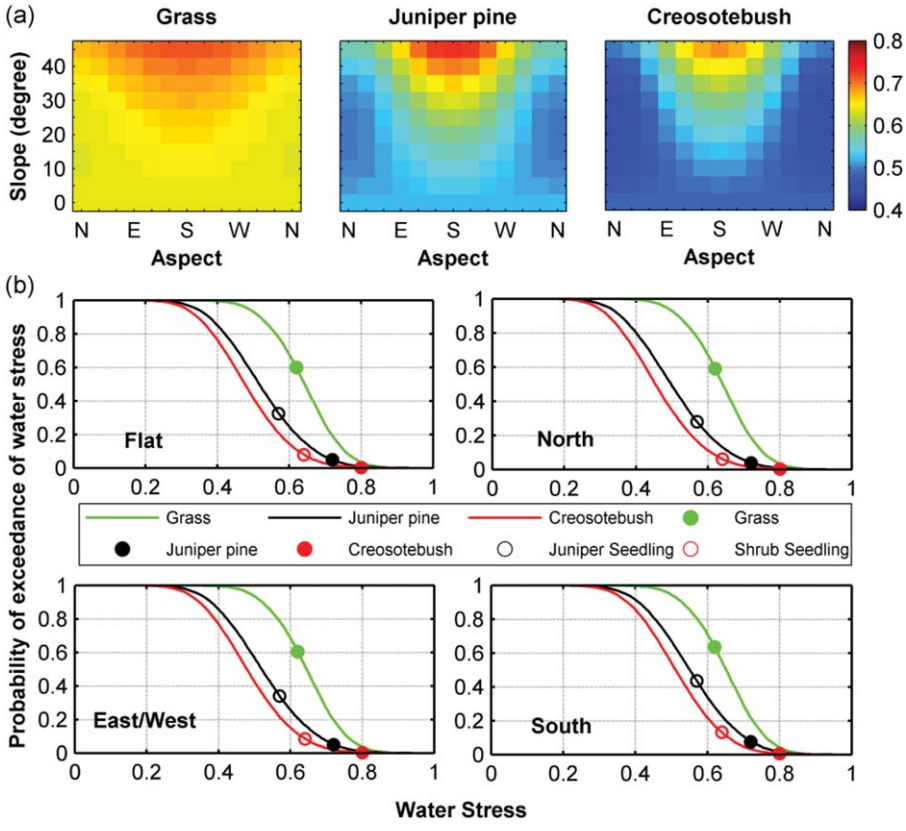

Figure 6. Base run: (a) mean annual normalized cumulative plant WS for grass, juniper pine, and creosotebush for different slope and aspect combinations; (b) probability of exceedance of mean annual WS for four major aspects and flat surface. Circles indicate drought resistance thresholds (θ) for each plant.

Bowen ratio tower; or other errors in rainfall measurement, especially in 1998 when ET was measured in absence of rain. Because of these uncertainties, we have not done a one-to-one comparison between the modeled and estimated evapotranspiration rates from the Bowen ratio tower.

[76] The MODIS LAI consistently gives 0.1 in the winter and 0.2 in the spring before the growing season at this site, which could arguably be an artifact of the algorithm used for calculating LAI (Figure 5d). Therefore, as the basis of our model comparison, we focus on the periods when MODIS LAI is larger than 0.2. The model shows consistency in estimating the onset of the growing and dormant seasons except for 2003, the driest year in the simulations, while the peak LAI is overestimated in some years. In order to assess model capability, the modeled LAI is plotted against MODIS-LAI (larger than 0.2) during the growing seasons (Figure 5e). Given that no calibration is performed using local ecohydrologic data, the result shows that CATGraSS could reasonably capture the local ecohydrological dynamics of grass. However, the accuracy of modeling LAI is lower than that of soil moisture when comparing their values of SEE and NSE, which might be caused by the lack of calibration, and the lower temporal and spatial resolution of the MODIS data. Future model confirmation studies should include local calibration for grass and additional validation for shrubs and trees.

5.1.2. Aspect Influence on Water Stress

[77] Before getting to the landscape level results, we illustrate the role of topography by plotting WS (equation (17b)) as a function of slope and aspect by averaging 10,000 years of model outputs for each of the 118 slope and aspect (S-A) classes (Figure 6a). It should be noted that all PFTs were placed in all S-A groups for comparison. Among the three PFTs, the modeled mean annual water stress is in the following order, from high to low: grass ($WS_G = 0.66$), juniper pine ($WS_T = 0.57$), and creosotebush ($WS_{SH} = 0.51$) averaged across the S-A domain (Figure 6a). As water stress is primarily defined as a function of soil moisture [e.g., *Porporato et al.*, 2001], the modeled water stress values reflect differences in plant rooting depth, soil moisture retention parameters (s^* and s_w), and the maximum transpiration rate (T_{max}). For a fixed rooting depth, under identical rainfall input, water stress grows with T_{max}. Among the three PFTs, creosotebush has the lowest T_{max} ($\overline{T}_{max\text{-}F\text{-}SH} = 3.77$ mm/d) and an intermediate rooting depth, leading to the lowest WS ($WS_{SH} = 0.51$). Juniper pine has higher T_{max} ($\overline{T}_{max\text{-}F\text{-}T} = 5.15$ mm/d), and deeper roots than the other two plant types. Even though T_{max} for grass is smaller than that of juniper pine ($\overline{T}_{max\text{-}F\text{-}T} = 4.96$ mm/d), shallower roots of grasses lead to the highest WS ($WS_G = 0.66$) among all PFTs.

[78] The role of topographic position is more pronounced in Figure 6a for juniper pine and creosotebush than grass. Water stress for grasses shows a relatively small range (0.64–0.72), with higher (lower) values corresponding to steep south facing (shallow north facing) slopes. Values of WS_G are nearly identical when slopes are less than

10°. Lack of strong aspect influence on grass water stress suggest that grasses could grow opportunistically everywhere in the basin where space is available. Increase in plant water stress with aspect from north to south, for a given slope, can be related to the simulated f_R and $f_{T\text{-}G}$ patterns (Figures 4b and 4c). Water stress grows with slope angle dramatically on south facing slopes for all PFTs. In the east-, west-, and south facing slopes, juniper pine shows the greatest increase in water stress as slope steepens, while high water stress value of creosotebush is only confined to steep south facing slopes. In shallow-to-moderate slopes in all aspects, juniper pine shows larger water stress than creosotebush.

[79] To quantitatively illustrate the role of aspect on water stress in the modeled catchment, we plot the probability of exceedance of mean annual WS (equation (17b)) for different aspects and a flat surface (Figure 6b). Circles indicate the calibrated drought resistance thresholds (θ) for each plant, which can be used to directly estimate the probability of exceedance of a given θ, $P(\mathrm{WS}\geq\theta)$. In practical sense, this indicates the fraction of time during plant life that it will experience water stress higher than its drought-resistance threshold, which would lead to a nonzero probability of mortality due to drought stress (equation (22)).

[80] For the entire S-A domain, $P(\mathrm{WS}\geq\theta)$ ranks from low to high in the order of creosotebush, juniper pine, creosotebush seedling, juniper pine seedling, and grass for all aspects in the domain. $P(\mathrm{WS}\geq\theta_G)$ for north- and south facing slopes are nearly identical (0.61 and 0.65, respectively). In contrast, the $P(\mathrm{WS}\geq\theta)$ for juniper pine and creosotebush seedlings on south facing slopes are up to twice as high as their $P(\mathrm{WS}\geq\theta)$ on north facing slopes. Mature creosotebush and juniper pine have relatively low $P(\mathrm{WS}\geq\theta)$. East- and west facing slopes and flat terrain behave nearly identical in terms of their water stress.

[81] These results clearly illustrate the drought resistant nature of creosotebush. If plant selection were to be only based on water stress minimization in nature, creosotebush would have dominantly occupied all topographic positions in this region. However, the observed plant distribution in the site with an aspect-controlled ecotone (Figure 3a) suggests that differences in plant life history (mortality, establishment), and seed dispersal strategies could be playing a significant role in the region, as will be addressed in the model simulations.

5.1.3. Spatial Patterns

[82] Maps of PFTs distribution from the base run with a 5 m by 5 m vegetation cell size at the end of 2000 (high-tree population year), 4000 (high-shrub population year), and 10,000 years, and the time series of plant cover percentages (% of cells occupied by a certain plant in the model domain) following each storm are presented in Figure 7. CATGraSS predictions, in general, agree with field observations: juniper pines and grasses coexist on north facing slopes, and creosotebush, with limited grass, dominate south facing slopes. The base run was also conducted using a 2.5 m by 2.5 m vegetation grid, which yielded generally consistent results both with respect to vegetation patterns and their cover fractions with the courser run reported in Figure 7. A limited comparison between the two runs will be presented in Figure 8.

[83] The coverage percentages of PFTs are dynamic, even under a stationary climate, and behave markedly different over time. The highly variable nature of grass fraction is typically driven by the interannual fluctuations in precipitation. Because grasses have overall higher water stress and lower drought resistance, they not only die back rapidly during dry yearsbut also grow back quickly in the following wetter years, as their seeds are assumed to be available at all locations. In addition, the establishment and mortality of grasses depends on rainfall of that year, which is characterized by strong interannual variability. In contrast, the establishment of creosotebush and juniper pine tree seedlings depends on the population of the parent plants in the area, building a significant memory in the historical precipitation magnitudes that trigger seedling establishment and a healthy growth.

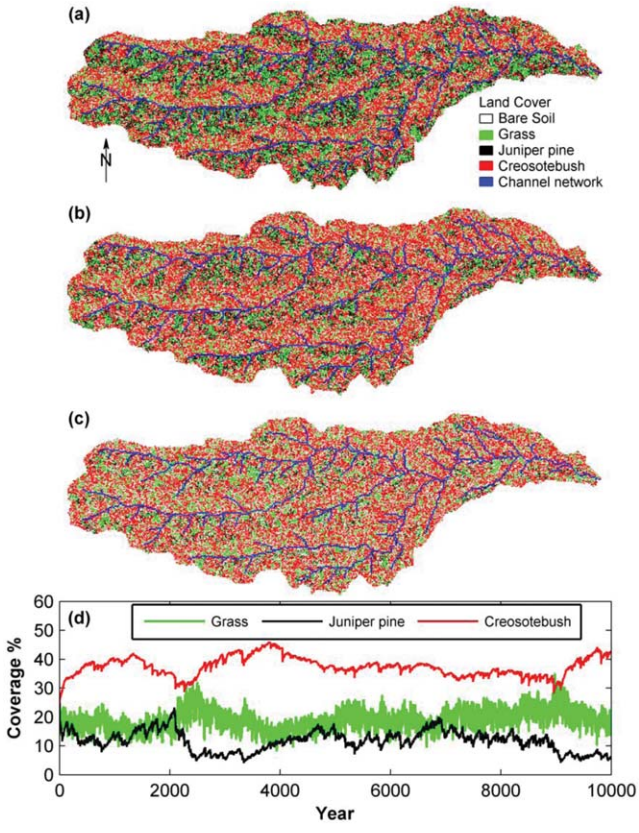

Figure 7. Base run: Simulated plant distribution of the study domain at years: (a) 2000, (b) 4000, and (c) 10,000, respectively, and (d) time series of percent coverage of PFTs in the catchment.

[84] Compared with grass vegetation, the areal coverage of creosotebush and juniper pine shows strong persistence over time and slower temporal dynamics. With the highest drought resistance (θ) and lowest WS (Figure 6), creosotebush experiences the least drought-induced mortality among the three PFTs, leading to a relatively constant and stable coverage over the simulation period (Figure 7d). This could be supported by the field data of *Bowers et al.* [1995], who showed that in the last 100 years, 84 out of 85 monitored creosotebush plants have survived at a Grand Canyon site despite periodic droughts. Ranked second in water stress and drought resistance, juniper pine experiences higher (lower) probability of drought-induced mortality

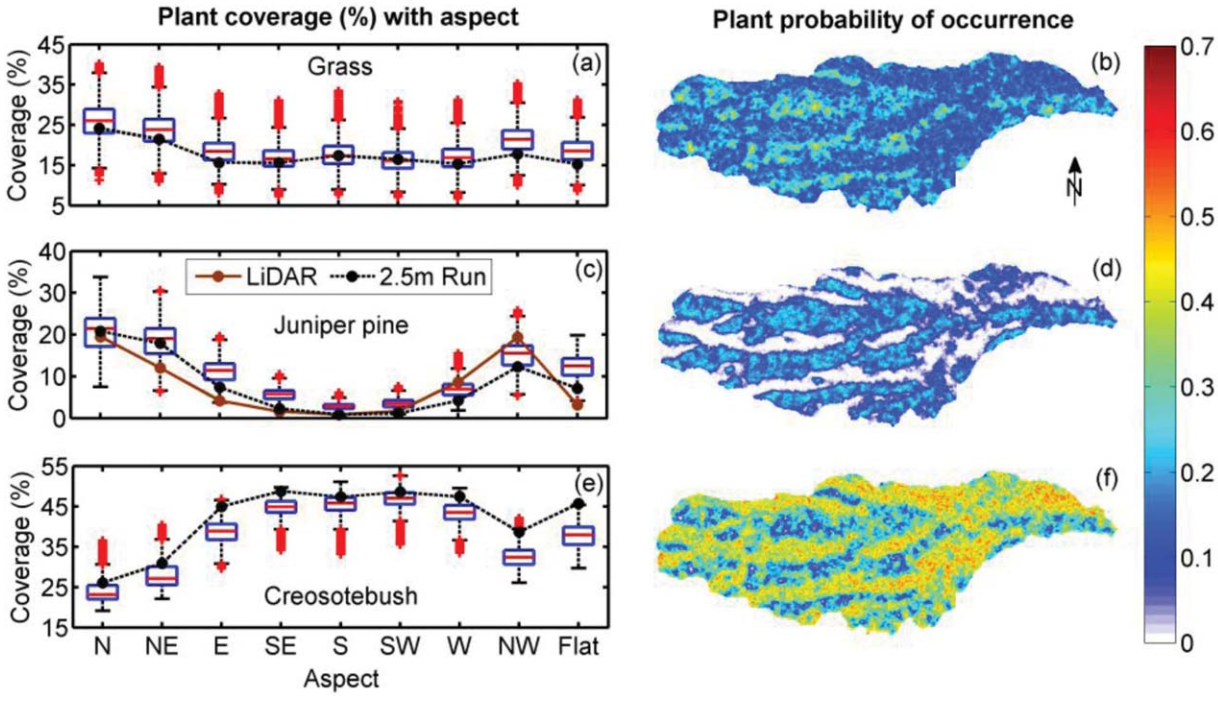

Figure 8. Model results for the base run: (left) percent plant coverage with respect to aspect and (right) plant probability of occurrence (PO) for (a, b) grass, (c, d) juniper pine, and (e, f) creosotebush. In the box-whisker plots, the red central line is the median, the edges of the box are the 25th and 75th percentiles, the whiskers extend to the most extreme data points not considered outliers, and outliers are plotted as red crosses. The dotted black dash line in Figures 8a, 8c, and 8e are the mean plant coverage with respect to aspect from a model run with 2.5 m by 2.5 m grid cells resolution. The dotted brown line in Figure 8c represents the juniper pine coverage derived from LiDAR data.

than that of creosotebush (grass). In wetter years, the two-ring seed dispersal strategy gives juniper an advantage (disadvantage) in seedling colonization as compared to creosotebush (grass). As a result, the coverage of juniper shows more (less) temporal dynamics than that of shrub (grass). Overall, juniper pine coverage exhibits persistence, with multicentury trends under the selected model parameters.

[85] Though the plant distribution map gives a general sense of aspect control on plant patterns (Figures 7a–7c); the role of topography can be better viewed by plotting, for all PFTs, the annual percent cover fractions with respect to aspect, and the probability of their occurrence (PO) over the modeled domain over time (Figure 8). PO is defined as the number of years a specific PFT existed on a cell, divided by the duration of the simulation. To generate this map, the model output from the last 5000 years of the simulation is used, since it shows a relatively stable behavior. In Figures 8a, 8c, and 8e (left), for each PFT, we present box-whisker plots of the annual percent coverage of a PFT with respect to each aspect group, and a map of their PO (right). To illustrate the role of vegetation grid cell resolution in Figures 8a, 8c, and 8e, the spatiotemporal average of plant coverage (%) are plotted for the finer resolution (2.5 m by 2.5 m) run.

[86] From north to south aspects in Figure 8 (left), the modeled dominant plant type changes from juniper pine to creosotebush (Figures 8c and 8e), while grass population decreases by about 10% (Figure 7a). Juniper pine almost exclusively exists on north facing slopes. The existing juniper pine percentages in the field, obtained from the LiDAR data, falls within the range of the modeled annual cover percentages of juniper pine in a given aspect (Figure 8c). Lack of fluctuations of creosotebush in the time series plot (Figure 7d) manifests itself with a low range in the box-whisker plots (Figure 8e) for all aspect groups. With the least water stress and highest drought resistant, creosotebush outcompetes the other two PFTs, and gains the highest PO on south aspects (Figure 8f). Grass shows a muted response to aspect (Figure 8a), which can be attributed to its relatively uniform water stress across the domain (Figure 6a). While grasses can grow in all aspects, albeit under stress, the reduced grass cover percentage on south facing slopes is a result of the allelopathic influence of shrubs on grasses. *McMahon* [1998] reported grass cover of 14% on south and 21% on north facing slopes in a headwater catchment of our study basin. These cover fractions are within the range simulated by the model (Figure 8a).

[87] The vegetation coverage-aspect relations for the two simulations that used different grid resolution are generally consistent with each other (Figures 8a, 8c, and 8e). For grass and tree vegetation, the spatiotemporal mean plant coverage (%) of the finer simulation, for a given aspect group, is within the 25th and 75th percentiles, and often falls on the median, of the annual spatial mean coverage represented in the box-whisker plot of the courser simulation. The finer vegetation size, however, supports a slight increase in the coverage of shrubs on all hillslope aspects.

[88] The model results presented above are not sensitive to the initial condition used for spatial plant distribution. The influence of initial vegetation pattern was tested by conducting 10 numerical experiments with CATGraSS in which the model was started with a different random vegetation distribution, but with the same probability of assignments for all PFTs and bare soil (25%). In the simulations, we observed that the model forgets the initial condition within the first thousand year, during which aspect-driven vegetation organization emerges on the landscape.

[89] It is interesting to see the role of plant life cycle in the simulations. In all aspects, creosotebush exhibits the lowest WS and the probability of mortality (P_M), and the highest live index. A plant selection procedure based on water stress minimization would have selected creosotebush in the entire basin. However, the success of juniper pine establishment in north facing slopes can be attributed to the longer seed dispersal range of juniper pines that enhance their probability of establishment in the model (equation (20c)) and their longevity. To test the role of seed dispersal range, we set up a model run in which we assumed juniper pines only send seeds to their immediate neighbors (first ring, as in creosotebush, instead of the double ring assumption). This led to an extinction of juniper pine species in the model (not shown). The finding shows that when the seed dispersal range is identical for both woody plants, creosotebush with a lower water stress and the allelopathic effect becomes more competitive and will drive juniper pine away. On the other hand, increasing the diameter of seed dispersal of juniper pines to more than two rings also increased the long-term average cover fraction of juniper pine to ~30% in the domain. Our result is consistent with other modeling studies that showed enhanced tree dominance over the domain as a result of increase in tree seed dispersal length [*Fernandez-Illescas and Rodriguez-Iturbe*, 2004].

[90] Although the emphasis of this paper is the role of aspect in vegetation patterns, the calibrated model predicts plant biomass consistent with observations. The modeled annual aboveground net primary productivity (ANPP, g DM m^{-2}) for grass ranges from 100 to 250 g DM m^{-2} with a mean of 160 g DM m^{-2}, consistent with some field studies in the SNWR that report 10 years ANPP data in the 170–200 g DM m^{-2} range [*Knapp and Smith*, 2001]. Modeled ANPP of creosotebush varies between 40 and 100 g DM m^{-2} (average of 66 g DM m^{-2}), about 10% higher than values reported by *Muldavin et al*. [2008] in the SNWR that has an average of 59.2 g DM m^{-2}. Modeled ANPP for juniper pine ranges from 60 to 175 g DM m^{-2} (average of 108 g DM m^{-2}). In a pinon-juniper savanna site (labeled Savanna in Figure 2), whose elevation is 1790 m ASL and MAP is 290 mm/yr, *Allen et al*. [2010] reported an average ANPP of 55 g C m^{-2} yr^{-1} for pinon-juniper woodland. This value can be converted to ~110 g DM m^{-2} yr^{-1} by using 2.0 as the conversion factor of carbon to dry matter for woody plants [*Ajtay et al*., 1979], which is about the same as the value predicted by the model.

5.2. Flat Run

[91] While the model captures the observed model patterns in the study sites, the critical question now is: Can the model successfully capture the observed vegetation patterns on flat terrain? We ran the model by setting the elevations in the whole catchment to the value of the outlet, using the identical rainfall sequencing, and the initial condition for PFT distribution. This numerical experiment produced a creosotebush dominant ecosystem with scattered patches of coexisting juniper pines and grasses (Figure 9). This model result is consistent with our observations. A photograph taken at about 2 mi east of the basin shows creosotebush dominance, clumps of grasses, and a juniper tree (Figure 3d) However, there are also sites within the SNWR characterized as grasslands and grass-to-shrubland transition zones (Figure 2c) [e.g., *D'Odorico et al*., 2010], which may be related to limited seed sources, rainfall differences and its interannual variability, grazing, and local disturbance such as fires, leading to a range of different plant assemblages [*Gosz et al*., 1995].

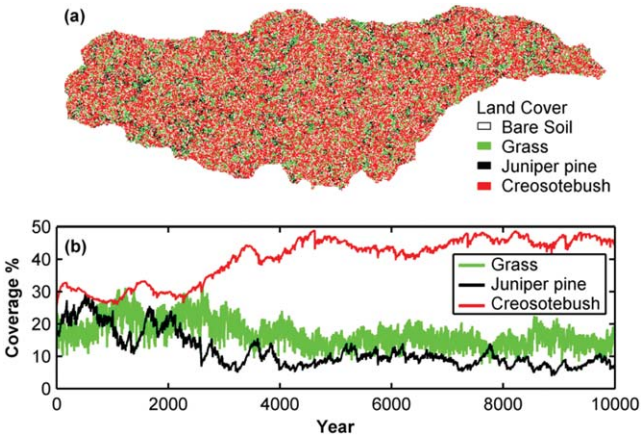

Figure 9. Flat surface run: (a) map of plant distribution in the final year of the simulation and (b) time series of percent coverage of PFTs throughout the simulation.

[92] In Table 5, we report the mean annual water balance components and the ANPP of the simulations, based on the final vegetation map. The basin-averaged annual ANPP of the base run (~67 g DM m^{-2} yr^{-1}) is only ~5% higher than that for the flat surface (~64 g DM m^{-2} yr^{-1}). This result indicates that based on the final model output, instead of increasing the ANPP of the domain, the topography leads to increased plant diversity, with only a subtle increase in ET/P and ANPP.

5.3. Model Sensitivity to Rainfall Frequency (Magnitude) and Seasonality

[93] Growing extremes is among the projected climate change scenarios in the southwest United States [*Wang*, 2005; *Diffenbaugh et al*., 2005], while the net change in the MAP is highly uncertain [*Seager et al*., 2007]. A simple way to represent growing extremes and shifting of monsoon season in the PRP model is to change the rainfall frequency and seasonality. Instead of applying the time series of climate change projection into our model, our main goal is to explore the model sensitivity to climatic forcing. Four experimental runs are performed: 20% increase and decrease of the mean time between storms (T_b), a stronger monsoon by increasing (decreasing) the wet (dry) season total rainfall by 50%, and a weakened effect of monsoon by removing seasonality in the model (same amount of rainfall for each month). All experimental runs keep the MAP

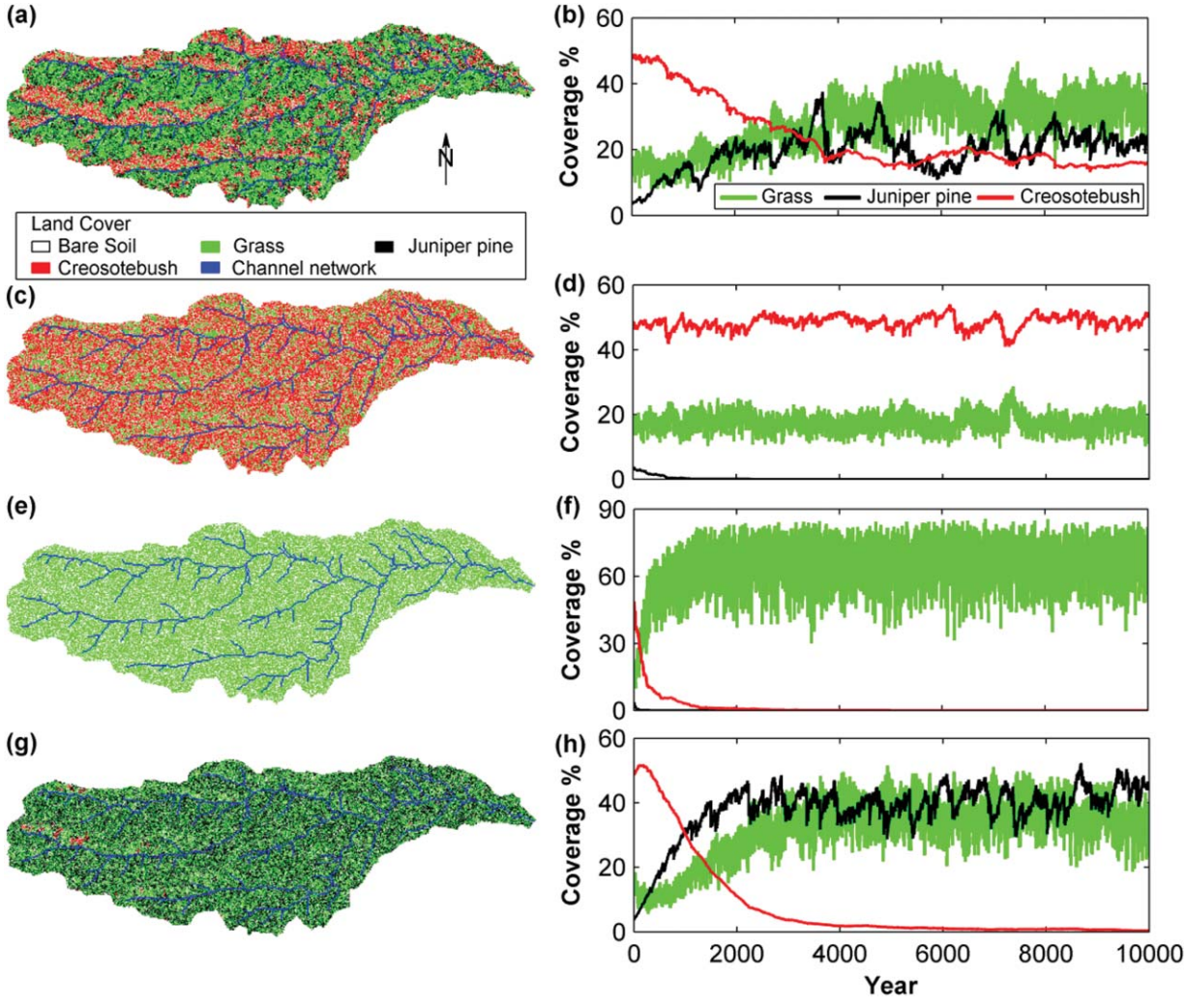

Figure 10. Model results of sensitivity runs: a map of plant distribution in the final year of the simulation, and time series of percent coverage of PFTs throughout the simulation for: (a, b) increase in mean time between storms (+20% T_b); (c, d) decrease in mean time between storms (−20% T_b); (e, f) enhanced monsoon precipitation (+50% increase); and (g, h) uniform climate (no monsoon).

constant at 250 mm/yr and are initialized by the final vegetation output of the base run (Figure 6c).

[94] In CATGraSS, a 20% increase in T_b under a constant MAP leads to less frequent storm events with higher magnitudes. Under this scenario, the mean annual water stress was reduced by all three PFTs by more fully recharging the root-zone soil moisture reservoir, consistent with some earlier field [e.g., *Knapp et al*., 2008] and modeling studies in semiarid climates [*Laio et al*., 2001; *Istanbulluoglu and Bras*, 2006]. Juniper pine trees with deeper roots got the highest absolute benefit from larger storm pulses ($\Delta WS_T = -0.029$, from 0.57), followed by creosotebush ($\Delta WS_{SH} = -0.025$, from 0.51) and grass ($\Delta WS_G = -0.013$, from 0.66) vegetation types. Higher establishment (equation (20c)) and lower drought-induced mortality probabilities (equation (22)) for juniper pine led to the expansion of trees in the simulated domain at the expense of creosotebush (Figures 10a and 10b). In the lower half of the basin toward the outlet where topography is less pronounced, creosotebush almost entirely disappeared. Grasses also benefit from the expansion of trees, as they only have a chance to occupy empty spaces away from the allelopathic influence of shrubs. With lower-frequency and higher-magnitude storms, supporting tree expansion, ANPP grew significantly (~97 g DM m^{-2} yr^{-1}), while (R+D)/P and ET/P remained relatively constant (Table 5). This can be explained by the increased coverage of juniper pine and grass species, with higher WUE than creosotebush (Table 3), leading to a larger gain of ANPP under the same ET loss (equation (12)).

[95] When T_b is decreased 20%, the amount of soil moisture in the root zone declined throughout the year, leading to higher WS in all PFTs studied. In the simulated domain, the basin-averaged increase of WS from low to high was in the order of grass ($\Delta WS_G = 0.01$, from 0.66), creosotebush ($\Delta WS_{SH} = 0.034$, from 0.51), and juniper pine ($\Delta WS_T = 0.043$, from 0.57). This result indicates that the depth-averaged soil moisture in the root zone remained below s^* for a longer duration in juniper pine than grass and creosotebush. Besides having deeper roots over which

the soil moisture is distributed, having a larger canopy interception capacity, that reduces the amount of water available for infiltration, contributed to the increased water stress levels for juniper pine in the model. Water stress induced mortality led to the complete loss of trees in the domain. With a higher drought tolerance than grasses, creosotebush became the dominant plant type as storms became more frequent, but delivered less rain (Figures 10c and 10d).

[96] We explore the implications of a stronger monsoon by increasing (decreasing) the wet (dry) season total rainfall by 50%, leading to an equivalent of 75% MAP falling in the monsoon season. Under this enhanced rainfall seasonality scenario, annual water stress grew for all PFTs. The largest increase in water stress is modeled for creosotebush, followed by juniper pine, and the smallest for grass. This can be related to two major causes in the system. First, a stronger monsoon (increased P_w) markedly increases runoff and leakage losses (Table 5), leaving less soil moisture storage for ET, and thus biomass production. Second, lower rainfall amounts in the dry season led to very low soil moisture levels, which negatively influenced juniper pine and creosotebush as they can transpire during the dry season, though at reduced rates. Grasses suffered the least from this scenario since the strengthened monsoon occurs during their growing season. As a result, grasses expanded in the region relatively rapidly following increased monsoon rainfall, while juniper pine and creosotebush died off (Figures 10e and 10f). In this simulation, 75% of MAP gives ~180 mm of rain in 3 months of the monsoon, bringing the amount of rain comparable with the summer rainfall in the dryer portions of the grasslands in the Nebraska Sand Hills [e.g., *Istanbulluoglu et al*., 2012].

[97] In order to explore a weakened effect of monsoon, we removed seasonality in the model and distributed rainfall evenly throughout the year. Interestingly, while water stress of grasses showed a small increase, water stress of both creosotebush and juniper pine dropped significantly. The greatest reduction in water stress was observed with juniper pine, which can accommodate and use the moisture from the winter in their deeper roots when the transpiration rate is low. Favored by climate, juniper pines rapidly extended to as high as 60% of the basin area (Figures 10g and 10h). We hypothesized that this could be related to the absence of creosotebush and the dominance of juniper pine in northern New Mexico, where NAM loses its strength. However, studies also have shown that cold temperature and the resulting freezing-induced cavitation could limit the geographical distribution of creosotebush [*Pockman and Sperry*, 1997].

[98] In Table 5, nearly all rainfall sensitivity simulation results show that more than 95% of the mean annual P was partitioned into ET, except for the increased wet-season precipitation scenario, in which ET was ~90% of P due to increased runoff/drainage loss. Monitoring ET fluxes at flat sites in the SNWR for three monsoon seasons from 2000 to 2002, *Kurc and Small* [2004] found ET ~95% of P in a grassland site and ~100% of P in a shrubland site. Comparison shows that vegetation patterns may have limited ability in modulating water balance in extreme arid regions, where the atmospheric ET demand goes far beyond P. Through influencing water stress, subtle differences in the spatial distribution of evapotranspiration demand over the landscape, however, will lead to vegetation separation with respect to aspect, as predicted by the model.

[99] It is critical to note that in all model simulations both creosotebush and juniper pine show a relatively slow temporal dynamics with respect to grasses. In the time series plots (Figures 7, 9, and 10), these two plants usually show a reciprocal behavior (as tree fraction decreases shrub fraction increases and vice versa). In the model, plant mortality is represented by a probability of death (equation (21)), which is a summation of the probabilities of death due to water stress, aging, and background disturbance. Both creosotebush and juniper pine have high longevity, meaning that under tolerable levels of climatic stress, their temporal dynamics would be mainly controlled by their lifespan and competition for space. As they remain alive in the model, they send seedlings to the environment that reinforce their coverage in the ecosystem. Because of their high drought resistance, unless a dramatic shift in climate is simulated, climate fluctuations have a relatively muted influence on creosotebush and juniper pine dynamics.

6. Discussion

[100] The optimality hypothesis of *Eagleson* [1982] argues that in water-limited ecosystems, optimal ecohydrologic conditions result from the minimization of canopy water stress. In a more general hypothesis, vegetation patterns observed in a range of water-limited ecosystems have been explored by means of a trade-off principal between resource consumption for growth and avoidance of water stress for survival [*Caylor et al*., 2009; *Franz et al*., 2010]. In the base run, water stress among the PFTs were ranked from low to high as: creosotebush, juniper pine, and grass in all topographic positions.

[101] At first glance, from a strict water stress minimization perspective, our findings could imply that the model results for the base run (and by inference the observed vegetation patterns) are inconsistent with the optimality hypothesis. In the model, NPP and the probability of establishment (P_E) are negatively related to, and the probability of drought-induced mortality (P_{Md}) is positively related to plant water stress. Creosotebush can grow in all aspect conditions, and due to their negligible P_{Md}, they die largely due to aging in all aspects. Junipers, on the other hand, show higher water stress and have lower drought-resistance threshold (θ), leading to a higher juniper P_{Md} than creosotebush (Figure 6b). In a highly competitive environment, the success of juniper pine establishment on north facing slopes can be solely attributed to their longer seed dispersal range in CATGraSS and the positive feedback between soil moisture and P_E. According to the current formulation of the model, a longer seed dispersal range could increase the number of seed sources surrounding a bare soil patch. Although the live index (equations (17a) and (17b)) of individual juniper pine trees could be overall smaller than that of neighboring creosotebush, when the mean live index of the community of each PFT is considered (equations (18) and (19)) to calculate P_E, juniper pine gains a competitive advantage against creosotebush on north facing slopes. Despite their lower drought resistance, higher water stress, and shorter longevity than creosotebush in the model

(and by inference, at the study site), having a longer dispersal range gives the juniper pine an advantage on north facing slopes over creosotebush. A simulation experiment that used the same dispersal range for both creosotebush and juniper pine (single ring) favored shrubs on north facing slopes, confirming this argument (simulation not shown).

[102] On the other hand, in the flat run, the increased dominance of shrubs supports Eagleson's optimality hypothesis [e.g., *Eagleson*, 1982]. Over the continuous and flat domain with spatially uniform rainfall and evapotranspiration forcing, various plant-specific life-history processes seemed to have a relatively "muted" role. Here juniper pine could not take advantage of their longer dispersal range because of the negative feedback between water stress, which is slightly higher on flat surface compared to a north facing slope, and P_E. As a result, creosotebush dominate the simulation domain, while junipers and grasses only survive in small-scale clusters.

[103] This paper did not intend to explore the optimality/trade-off hypothesis any further detail. However, our findings maybe couched in the context of a trade-off-based hypothesis [*Caylor et al*., 2009; *Franz et al*., 2010]. In the base run, despite water stress is not minimized at the landscape scale due to juniper pine-grass coexistence on north facing slopes, runoff production decreased, ANPP grew by a slight margin compared to the flat run where shrubs dominate, and the landscape became ecologically more diverse. It could be argued that the ways in which different PFTs respond to water stress highly vary at different levels of water stress and are tightly related to how efficient different plants are in using water for life processes. As such, organization of vegetation in water-limited ecosystems could be a result of ecohydrological trade-offs involving processes of plant competition for space and resources that lead to highly diverse ecosystems. Most of these processes are not yet explicitly represented in numerical models of ecohydrology, and the existing models and theory cannot accurately quantify the benefits of ecologic diversity. We anticipate that more generalized hypothesis explaining the organization of plant patterns will emerge with advances in numerical models of ecohydrological organization that can address complexity and feedbacks loops in highly diverse ecosystems, and advanced remote sensing, and field observational technologies for plant response.

[104] Two other model assumptions that had critical influence on the simulated plant patterns are the assumptions regarding the abundance of grass seeds in the simulation domain and the allelopathic effect of creosotebush on grass growth. Taking advantage of the abundance of their seeds, grasses opportunistically grow in the model domain where trees and shrubs have limited establishment chances because of the absence of mature adults. The allelopathic effect of creosotebush significantly reduces the grass population in their neighboring cells. The manifestations of both of these assumptions can be clearly seen in the model results, two of which are provided as examples. First, without the allelopathic effect of shrubs, grass growth would only be limited to grass water stress, which does not significantly vary with aspect, for the range of slopes ($<25°$) observed in our study catchment (Figure 6a). Therefore, without the allelopathic effect of creosotebush on grass, grasses would likely to grow on south facing slopes nearly as much as they grow on north facing slopes. Second, changes in the grass-covered aspects from north to south facing slopes as trees died off in the 20% reduced T_b simulation (Figures 10c and 10d) clearly shows the capacity of shrubs to outcompete grasses on north facing slopes, and the ability of grasses to quickly occupy south facing aspects, as shrubs died as a result of increased water stress.

[106] While the vegetation pattern simulated by the CATGraSS model showed good agreement with field observation, the model is still a preliminary step toward understanding the complex topography-vegetation coupling under semiarid climate. Some of the major limitations of this model are discussed in order. First of all, the single-layer, depth-averaged soil moisture balance model neglects the lateral subsurface moisture transfer and runoff/run-on processes that occur during the summer flood events in SNWR [*Gutiérrez-Jurado et al*., 2007; *Turnbull et al*., 2010] or in the winter [*McCord and Stephens*, 1987]. This simplification may constrain our ability to fully examine the role of topography on the ecohydrology of semiarid ecosystems [*Ivanov et al*., 2008a, 2008b; *Franz et al*., 2012]. Secondly, the uniformity in soil texture and rainfall fails to capture resource variability in the modeled vegetation patterns. Higher organic matter content and finer soil texture has been reported for the north facing slopes in the study catchment [*McMahon* 1998; *Gutiérrez-Jurado et al*., 2006]. Summer rainfall events vary spatially in the SNWR [e.g., *Gosz et al*., 1995], and rainfall amount may follow along with elevation gradient within our study basin, which was not represented in CATGraSS.

[107] Third, the model does not represent the role of nutrients, which no doubt have a critical role in plant growth even in semiarid ecosystems [*Porporato et al*., 2003]. Incorporating nutrient dynamics in this model would allow predict the growth and establishment rates of plants in more ecologically sound ways. In particular, in modeling ecosystems with strong aspect control, incorporating nutrient dynamics will allow to represent the differences in nutrient levels of opposing hillslope aspects under different plant types, which could have strong feedbacks on vegetation growth, the resilience of topography-controlled ecosystem patterns, and the critical zone processes.

[108] We feel that the greatest limitation of CATGraSS and the component that needs a field-based validation and future improvements is the procedure used to assign a plant type on an empty cell, which is purely based on conjecture, that involves the definition of a seed dispersal range, plant wellness index, and a probabilistic plant selection criteria. This rule set controls the rate of plant colonization at empty sites and commands the landscape-scale response to changes in climate and wildfire regime and human impact. The influence of grid spatial resolution for modeling the cellular-automata plant dynamics on model predictions also remains to be a critical issue that needs to be further explored. The limited sensitivity analysis we showed by changing the vegetation grid resolution to 2.5 m (from 5 m) did not have a very significant influence on the simulated vegetation distribution. Seed dispersal lengths for trees and shrubs should also be adjusted consistent with the vegetation cell resolution, as in the current model the seed dispersal range is measured by the number of cells seeds can travel.

[109] CATGraSS would greatly benefit from a test of predicting vegetation change in the observed ecological history of the southwest United States. The great majority of the region has been undergoing dramatic vegetation shifts, triggers of which have not been entirely understood. For example, in a Texas savanna, *Archer et al*. [1988] documented increase in the total woody plant coverage from 8% in 1960 to 36% in 1983, triggered by a serious of wetter-than-average growing seasons. The nearly fourfold increase in tree coverage indicates a rather quick expansion of woody plants. In our study site, however, both creosotebush and juniper pine are highly drought-resistant plants as shown in our model result and field data [e.g., *Bowers et al*., 1995]. Thus, both creosotebush and juniper pine trees show a relatively slow temporal response in CATGraSS. The probabilistic colonization component of CATGraSS can also be responsible for a slow response of the plant coverage in the model over time to climate. Therefore, in order to capture rapid changes of vegetation distribution at regional scale, it is critical to parameterize and calibrate models with local climate data and plant properties. Also, studies show that other factors, not currently included in CATGraSS, such as the role of soil nutrients, fire frequency changes, grazing pressure, and seed dispersal by animals, may also contribute to the vegetation response under climate change [e.g., *Buffington and Herbel*, 1965; *Scholes and Archer*, 1997; *Van Auken*, 2009].

[110] CATGraSS was calibrated manually to obtain a set of deterministic model parameters. The model parameters used to simulate soil moisture and vegetation dynamics lie within the ranges of reasonable values reported in the literature, and in some cases are taken directly from field work and prior modeling efforts (Table 2). It is plausible that a set of different values of the model parameters used could potentially produce similar results. However, for the purposes of this study, we find that the parameter set used was realistic for the simulation experiments carried out and the findings emanating from them. We have recognized in this paper that the CA parameters used to simulate plant establishment and mortality (Table 4) are most uncertain. Consequently, those parameters have been selected in consistence with *van Wijk and Rodriguez-Iturbe* [2002] through a multitude of model simulation experiments, and the model response to their variation have been discussed qualitatively in this paper. We specifically encourage future studies to examine the cellular automaton parameters presented in Table 4 through additional model sensitivity analysis and focused case studies that would involve historical change characterized by aerial photography and remote sensing data.

7. Summary and Conclusion

[111] In this paper, we present a Cellular Automata Tree-Grass-Shrub Simulator (CATGraSS) for modeling the dynamics of tree, grass, and shrub plant types in water-limited ecosystems. In the model, the incoming shortwave radiation and maximum evapotranspiration were treated spatially explicit on the terrain using a DEM. Plant competition for space is modeled using a probability of plant establishment, driven by plant water stress, and seed dispersal lengths. Plant mortality was defined based on three factors: plant age, cumulative water stress in excess of a drought resistance threshold, and a background mortality rate. CATGraSS was tested in central New Mexico in a catchment characterized by an aspect-driven ecotone shift from a juniper-grass savanna on North (N) facing slopes to a creosotebush-dominated ecosystem on South (S) facing slopes. Forced by a stochastic representation of the current climate, the calibrated model run on actual catchment topography (base run) predicted the observed plant patterns and their cover fractions in relation to hillslope aspect reasonably well. CATGraSS run on a flat domain showed creosotebush dominance, with scattered random patches of tree-grass coexistence, consistent with observed plant patterns on flat landscapes of the study region.

[112] Climate change and growing natural and anthropogenic ecosystem disturbances present prediction challenges of the response of ecohydrologic systems with coexisting PFTs. In regions with relatively uniform topography, soils, and climate the spatial distribution of resources on the landscape can be considered relatively uniform. In such conditions, perhaps spatially lumped models of plant coexistence can be used for predicting vegetation dynamics and regional water balance. However, under pronounced topography, where soil moisture distribution is related to hillslope aspect, spatially explicit modeling would be critical to examine the future response of vegetation patterns under change, and when the implications of vegetation change on hillslope erosion, soil development, and other critical zone processes are of interest. Spatially explicit modeling of plant dynamics also presents tremendous opportunities for improved predictions of shifts in ecosystem boundaries and the rate and dynamics of ecosystem migration with climate change and anthropogenic disturbances.

[113] **Acknowledgments.** This work is supported by NSF grant EAR-0963858 and OCI-1148305. The authors thank Omer Yetemen, Homero Flores-Cervantes, Hugo Gutierréz-Jurado, Bruce J. Harrison, and Rafael L. Bras for their contributions. The authors thank the three anonymous reviewers and the Associated Editor for their constructive comments that improved the manuscript.

References

Accatino, F., C. De Michele, R. Vezzoli, D. Donzelli, and R. J. Scholes (2010), Tree-grass co-existence in savanna: Interactions of rain and fire, *J. Theor. Biol.*, *267*, 235–242.

Ajtay, G. L., P. Ketner, and P. Duvigneaud (1979), Terrestrial primary production and phytomass, in *The Global Carbon Cycle*, edited by B. Bolin et al., pp. 129–182, John Wiley, New York.

Allen, M. F., E. B. Allen, J. L. Lansing, K. S. Pregitzer, R. L. Hendrick, R. W. Ruess, and S. L. Collins (2010), Responses to chronic N fertilization of ectomycorrhizal piñon but not arbuscular mycorrhizal juniper in a piñon-juniper woodland, *J. Arid. Environ.*, *74*, 1170–1176.

Allen, R. G., L. S. Pereira, D. Raes, and M. Smith (1998), *Crop evapotranspiration: Guidelines for computing crop water requirements*, FAO Irrig. and Drain. Pap. 56, FAO, Rome, Italy.

Allen, R. G., R. Trezza, and M. Tasumi (2006), Analytical integrated functions for daily solar radiation on slopes, *Agric. For. Meteorol.*, *139*, 55–73.

Archer, S., C. Scifres, C. R. Bassham, and R. Maggio (1988), Autogenic succession in a subtropical savanna: Conversion of grassland to thorn woodland, *Ecol. Monogr.*, *58*(2), 111–127.

Arora, V. K. (2002), Modeling vegetation as a dynamic component in soil-vegetation-atmosphere transfer schemes and hydrological models, *Rev. Geophys.*, *40*(2), 1006, doi:10.1029/2001RG000103.

Arora, V. K., and G. J. Boer (2006), Simulating competition and coexistence between plant functional types in a dynamic vegetation model, *Earth Interact.*, *10*(10), 1–30.

Ayyad, M. A. G., and R. L. Dix (1964), An analysis of a vegetation-microenvironmental complex on prairie slopes in Saskatchewan, *Ecol. Monogr*, *34*, 421–442.

Baudena, M., F. D'Andrea, and A. Provenzale (2010), An idealized model for tree-grass coexistence in savannas: The role of life stage structure and fire disturbances, *J. Ecol.*, *98*, 74–80.

Beer, C., et al. (2010), Terrestrial gross carbon dioxide uptake: Global distribution and covariation with climate, *Science*, *329*, 834–838.

Bhark, E. W., and E. E. Small (2003), Association between plant canopies and the spatial patterns of infiltration in shrubland and grassland of the Chihuahuan desert, *New Mexico, Ecosystems*, *6*, 185–196.

Bonan, G. B., S. Levis, S. Sitch, M. Vertenstein, and K. W. Oleson (2003), A dynamic global vegetation model for use with climate models: Concepts and description of simulated vegetation dynamics, *Global Change Biol.*, *9*, 1543–1566.

Bowers, J. E., R. H. Webb, and R. J. Rondeau (1995), Longevity, recruitment and mortality of desert plants in Grand Canyon, USA, *J. Veg. Sci.*, *6*, 551–564.

Bras, R. L. (1990), *Hydrology. An Introduction to Hydrologic Science*, 1st ed., 643 pp., Addison-Wesley-Longman, Reading, Mass.

Breshears, D. D., P. M. Rich, F. J. Barnes, and K. Campbell (1997), Overstory-imposed heterogeneity and solar radiation and soil moisture in as semiarid woodland, *Ecol. Appl.*, *7*(4), 1201–1215.

Brolsma, R. J., and M. F. P. Bierkens (2007), Groundwater-soil water-vegetation dynamics in a temperate forest ecosystem along a slope, *Water Resour. Res.*, *43*, W01414, doi:10.1029/2005WR004696.

Buffington, L. C., and C. H. Herbel (1965), Vegetational changes on a semidesert grassland range from 1858 to 1963, *Ecol. Monogr.*, *35*(2), 139–164.

Campbell, G. S. (1974), A simple method for determining unsaturated conductivity from moisture retention data, *Soil Sci.*, *117*, 3311–3314.

Caylor, K. K., S. Manfreda, and I. Rodriguez-Iturbe (2005), On the coupled geomorphological and ecohydrological organization of river basins, *Adv. Water Resour.*, *28*(1), 69–86.

Caylor, K. K., T. M. Scanlon, and I. Rodriguez-Iturbe (2009), Ecohydrological optimization of pattern and processes in water-limited ecosystems: A trade-off-based hypothesis, *Water Resour. Res.*, *45*, W08407, doi:10.1029/2008WR007230.

Cayrol, P., A. Chehbouni, L. Kergoat, G. Dedieu, P. Mordelet, and Y. Nouvellon (2000), Grassland modeling and monitoring with SPOT-4 VEGETATION instrument during the 1997–1999 SALSA experiment, *Agric. For. Meteorol*, *105*, 91–115.

Chew, R. M., and A. E. Chew (1965), The primary productivity of a desert-shrub (Larrea tridentata) community, *Ecol. Monogr.*, *35*(4), 355–375.

Collatz, G. J., M. Ribas-Carbo, and J. A. Berry (1992), Coupled photosynthesis-stomatal conductance model for leaves of C4 plants, *Aust. J. Plant Physiol.*, *19*, 519–538.

Collins, D. B. G., and R. L. Bras (2010), Climatic and ecological controls of equilibrium drainage density, relief, and channel concavity in drylands, *Water Resour. Res.*, *46*, W04508, doi:10.1029/2009WR008615.

Couteron, P., and O. Lejeune (2001), Periodic spotted patterns in semi-arid vegetation explained by a propagation-inhibition model, *J. Ecol.*, *89*, 616–628.

Cox, P. M. (2001), *Description of the TRIFFID dynamic global vegetation model*, Hadley Centre Tech. Note 24, 16 pp., Hadley Centre, Bracknell, U. K.

Cramer, W., et al. (2001), Global response of terrestrial ecosystem structure and function to CO2 and climate change: Results from six dynamic global vegetation models, *Global Change Biol.*, *7*, 357–373.

de Reffye, P., T. Fourcaud, F. Blaise, D. Barthélémy, and F. Houllier (1997), A functional model of tree growth and tree architecture, *Silva Fennica*, *31*, 297–311.

Diffenbaugh, N. S., J. S. Pal, R. J. Trapp, and F. Giorgi (2005), Fine-scale processes regulate the response of extreme events to global climate change, *Proc. Natl. Acad. Sci. U. S. A.*, *102*(44), 15,774–15,778.

Dingman, S. L. (2002), *Physical Hydrology*, 2nd ed., Prentice Hall, Upper Saddle River, N. J.

D'Odorico, P., J. D. Fuentes, W. T. Pockman, S. L. Collins, Y. He, J. A. Medeiros, S. DeWekker, and M. E. Litvak (2010), Positive feedback between microclimate and shrub encroachment in the northern Chihuahuan desert, *Ecosphere*, *1*(6), art 17, doi:10.1890/ES10–00073.1.

Dunne, J. A., J. Harte, and K. J. Taylor (2003), Subalpine meadow flowering phenology responses to climate change: Integrating experimental and gradient methods, *Ecol. Monogr.*, *73*, 69–86.

Dyck, S. (1983), *Overview on the Present Status of the Concepts of Water Balance Model*, in New Approach in Water Balance Computations (Proceedings of the Hamburg Workshop), edited by A. Van der Beken and A. Herrmann, IAHS Publ. No. 148, pp. 3–19.

Eagleson, P. S. (1972), Dynamics of flood frequency, *Water Resour. Res.*, *8*(2), 878–898.

Eagleson, P. S. (1982), Ecological optimality in water-limited natural soil vegetation systems: 1. Theory and hypothesis, *Water Resour. Res.*, *18*(2), 325–340.

Eagleson, P. S., and R. I. Segarra (1985), Water-limited equilibrium of savanna vegetation systems, *Water Resour. Res.*, *21*, 1483–1493.

Emmerich, W. E. (2003), Carbon dioxide fluxes in a semiarid environment with high carbonate soils, *Agric. For. Meteorol.*, *116*, 91–102.

Escudero, A., M. J. Albert, A. J. M. Pita, and F. Perez-Garcia (2000), Inhibitory effects of Artemisia herba-alba on the germination of the gypsophyte Helianthemum squamatum, *Plant Ecol.*, *148*, 71–80.

Farquhar G. D., J. R. Ehleringer, and K. T. Hubick (1989), Carbon isotope discrimination and photosynthesis, *Annual Review of Plant Physiology and Plant Molecular Biology*, *40*, 503–537.

Fenner, M. (1987), Seedlings, *New Phytol.*, *106*, 35–47.

Fernandez-Illescas, C. P., and I. Rodriguez-Iturbe (2004), The impact of interannual rainfall variability on the spatial and temporal patterns of vegetation in a water-limited ecosystem, *Adv. Water Resour.*, *27*, 83–95.

Fowler, N. (1986), The role of competition in plant communities in arid and semiarid regions, *Annu. Rev. Ecol. System.*, *17*, 89–110.

Forzieri, G., F. Castelli, and E. R. Vivoni (2011), Vegetation dynamics within the North American monsoon region, *J. Clim.*, *24*(6), 1763–1783.

Friend, A. D. (1995), PGEN: An integrated model of leaf photosynthesis, transpiration, and conductance, *Ecol. Model.*, *77*, 233–255.

Franz, T. E., K. K. Caylor, J. M. Nordbotten, R. I. Rodriguez-Itubre, and M. A. Celia (2010), An ecohydrological approach to predicting regional woody species distribution patterns in dryland ecosystems, *Adv. Water Resour.*, *33*, 215–230, doi:10.1016/j.advwatres.2009.12.003.

Franz, T. E., K. K. Caylor, E. G. King, J. M. Nordbotten, M. A. Celia, and R. I. Rodriguez-Itubre (2012), An ecohydrological approach to predicting hillslope-scale vegetation patterns in dryland ecosystems, *Water Resour. Res.*, *48*, W01515, doi:10.1029/2011WR010524.

Gesch, D., M. Oimoen, S. Greenlee, C. Nelson, M. Steuck, and D. Tyler (2002), The national elevation dataset, *Photogramm. Eng. Remote Sens.*, *68*(1), 5–11.

Gosz, J. R., D. I. Moore, G. A. Shore, H. D. Grover, W. Rison, and C. Rison (1995), Lightning estimates of precipitation location and quantity on the Sevilleta LTER, *New Mexico, Ecol. Appl.*, *5*, 1141–1150.

Green, G. N., and G. E. Jones (1997), *The digital geologic map of New Mexico in ARC/INFO Format*, U.S. Geol. Surv. Open-File Rep. OFR 97-0052, U.S. Geol. Surv., Denver, Colo.

Grier C. C., K. J. Elliot, and D. G. McCullough (1992), Biomass distribution and productivity of Pinus edulis-Juniperus monosperma woodlands of north-central Arizona, *For. Ecol. Manage.*, *50*, 331–350.

Grunzweig, J. M., L. Tin, E. Rotenberg, A. Schwartz, and D. Yakir, (2003), Carbon sequestration in arid-land forest, *Global Change Biol.*, *9*, 791–799.

Guan, H., and J. L. Wilson (2009), A hybrid dual-source model for potential evaporation and transpiration partitioning, *J. Hydrol.*, *377*, 405–416.

Gutiérrez-Jurado, H. A., and E. R. Vivoni (2013), Ecogeomorphic expressions of an aspect-controlled semiarid basin: II. Topographic and vegetation controls on solar irradiance, *Ecohydrol.*, *6*, 24–37, doi:10.1002/eco.1263.

Gutiérrez-Jurado, H. A., E. R. Vivoni, J. B. J. Harrison, and H. Guan (2006), Ecohydrology of root zone water fluxes and soil development in complex semiarid rangelands, *Hydrol. Process.*, *20*, 3289–3316.

Gutiérrez-Jurado, H. A., E. R. Vivoni, E. Istanbulluoglu, and R. L. Bras (2007), Ecohydrological response to a geomorphically significant flood event in a semiarid catchment with contrasting ecosystems, *Geophys. Res. Lett.*, *34*, L24S25, doi:10.1029/2007GL030994.

Higgins, S. I., W. J. Bond, and W. S. W. Trollope (2000), Fire, resprouting and variability: A recipe for grass-tree coexistence in savanna, *J. Ecol.*, *88*, 213–229.

Hochberg, M. E., J. C. Menaut, and J. Gignoux (1994), The influence of tree biology and fire in the spatial structure of the West African savannah, *J. Ecol.*, *82*, 217–226.

House, J., S. Archer, D. D. Breshears, R. J. Scholes, and NCEAS Tree-Grass Interaction Participants (2003), Conundrums in mixed woody-herbaceous plant systems, *J. Biogeogr.*, *30*, 1763–1777.

Hwang, T., C. Song, J. M. Vose, and L. E. Band (2011), Topography-mediated controls on local vegetation phenology estimated from MODIS vegetation index, *Landscape Ecol.*, *26*, 541–556, doi:10.1007/s10980-011-9580-8.

Istanbulluoglu, E., and R. L. Bras (2006), On the dynamics of soil moisture, vegetation and erosion: Implications of climate variability and change, *Water Resour. Res.*, *42*, W06418, doi:10.1029/2005WR004113.

Istanbulluoglu, E., T. Wang, and D. A. Wedin (2012), Evaluation of ecohydrologic model parsimony at local and regional scales in a semiarid grassland ecosystem, *Ecohydrol.*, *5*, 121–142, doi:10.1002/eco.211.

Ivanov, V. Y., R. L. Bras, and D. C. Curtis (2007), A weather generator for hydrological, ecological, and agricultural applications, *Water Resour. Res.*, *43*, W10406, doi:10.1029/2006WR005364.

Ivanov, V. Y., R. L. Bras, and E. R. Vivoni (2008a), Vegetation-hydrology dynamics in complex terrain of semiarid areas: 1. A mechanistic approach to modeling dynamic feedbacks, *Water Resour. Res.*, *44*, W03429, doi:10.1029/2006WR005588.

Ivanov, V. Y., R. L. Bras, and E. R. Vivoni (2008b), Vegetation-hydrology dynamics in complex terrain of semiarid areas: 2. Energy-water controls of vegetation spatiotemporal dynamics and topographic niches of favorability, *Water Resour. Res.*, *44*, W03430, doi:10.1029/2006WR005595.

Jeltsch, F., G. E. Weber, and V. Grimm (2000), Ecological buffering mechanisms in savannas: A unifying theory of long-term tree–grass coexistence, *Plant Ecol.*, *150*, 161–171.

Jeltsch, F., S. J. Milton, W. R. J. Dean, and N. van Rooyen (1996), Tree spacing and coexistence in semi-arid savannas, *J. Ecol.*, *84*, 583–595.

Jeltsch, F., S. J. Milton, W. R. J. Dean, N. van Rooyen, and K. A. Moloney (1998), Modelling the impact of small-scale heterogeneities on tree-grass coexistence in semi-arid savannas, *J. Ecol.*, *86*(5), 780–793.

Johnsen, T. N. (1962), One-seed juniper invasion of Northern Arizona grasslands, *Ecol. Monogr.*, *32*, 187–207.

Kim, Y., and E. A. B. Eltahir (2004), Role of topography in facilitating coexistence of trees and grasses within Savannas, *Water Resour. Res.*, *40*, W07505, doi:10.1029/2003WR002578.

Klausmeier, C. A. (1999), Regular and irregular patterns in semiarid vegetation, *Science*, *284*, 1826–1828.

Knapp, A. K., and M. D. Smith (2001), Variation among biomes in temporal dynamics of aboveground primary production, *Science*, *291*, 481–484.

Knapp, A. K., et al. (2008), Consequences of more extreme precipitation regimes for terrestrial ecosystems, *BioSciences*, *58*, 811–821.

Knipe, D., and C. H. Herbel, (1966), Germination and growth of some semidesert grassland species treated with aqueous extract from creosotebush, *Ecology*, *47*(5), 775–781.

Kucharik, C. J., J. A. Foley, C. Delire, V. A. Fisher, M. T. Coe, J. D. Lenters, C. Young-Molling, N. Ramankutty, J. M. Norman, and S. T. Gower (2000), Testing the performance of a dynamic global ecosystem model: Water balance, carbon balance, and vegetation structure, *Global Biogeochem. Cycles*, *14*(3), 795–825.

Kurc, S. A., and E. E. Small (2004), Dynamics of evapotranspiration in semiarid grassland and shrubland during the summer monsoon season, central New Mexico, *Water Resour. Res.*, *40*, W09305, doi:10.1029/2004WR003068.

Laio, F., A. Porporato, L. Ridolfi, and I. Rodriguez-Iturbe (2001), Plants in water controlled ecosystems: Active role in hydrologic processes and response to water stress. II. Probabilistic soil moisture dynamics, *Adv. Water Resour.*, *24*, 707–723.

Lajtha, K., and J. Getz (1993), Photosynthesis and water-use efficiency in pinyon-juniper communities along an elevation gradient in northern New Mexico, *Oecologia*, *94*(1), 95–101.

Lajtha, K., and W. G. Whitford (1989), The effect of water and nitrogen amendments on photosynthesis, leaf demography, and resource-use efficiency in Larrea tridentata, a desert evergreen shrub, *Oecologia*, *80*(3), 341–348.

Larcher, W. (1995), *Physiological Plant Ecology*, 3rd ed., New York, Springer.

Lee, T. J. (1992), The impact of vegetation on the atmospheric boundary layer and convective storms, Ph.D. dissertation, 137 pp., Colorado State Univ., Fort Collins, Colo. (United States).

Lejeune, O., M. Tlidi, and P. Couteron (2002), Localized vegetation patches: A self-organized response to resource scarcity, *Phys. Rev. E*, *66*, 010901–1.

Martens, S. N., D. D. Breshears, and C. W. Meyer (2000), Spatial distributions of understory light along the grassland forest continuum: Effects of cover, height, and spatial pattern of tree canopies, *Ecol. Modell.*, *126*, 79–93.

McCord, J. T., and D. B. Stephens (1987), Lateral moisture flow beneath a sandy hillslope without an apparent impeding layer, *Hydrol. Process.*, *1*(3), 225–238.

McDowell, M., et al. (2008), Mechanisms of plant survival and mortality during drought: Why do some plants survive while others succumb drought? *New Phytol.*, *178*, 719–739.

McMahon, D. R. (1998), Soil, landscape and vegetation interactions in a small semi-arid drainage basin: Sevilleta National Wildlife Refuge, M.S. thesis, New Mexico Inst. of Mining and Technol., Socorro, N. M.

Molnar, P., and J. A. Ramirez, (2001), Recent trends in precipitation and streamflow in the Rio Puerco Basin, *J. Clim.*, *14*, 2317–2328.

Montaldo, N., R. Rondena, J. D. Albertson, and M. Mancini (2005), Parsimonious modeling of vegetation dynamics for ecohydrologic studies of water-limited ecosystems, *Water Resour. Res.*, *41*, W10416, doi:10.1029/2005WR004094.

Montaldo, N., J. D. Albertson, and M. Mancini (2008), Vegetation dynamics and soil water balance in a water-limited Mediterranean ecosystem on Sardinia, Italy, *Hydrol. Earth Syst. Sci. Discuss.*, *5*, 219–255.

Monteith, J. L. (1965), Evaporation and environment, *Symp. Soc. Exp. Biol.*, *19*, 205–224.

Moore, D. (1989−2008), Meteorological data on the Sevilleta National Wildlife Refuge, NewMexico. Sevilleta LTER database. [Available at http://sev.lternet.edu/project_details.php?id=SEV001.].

Muldavin, E. H., D. I. Moore, S. I. Collins, K. Wetherill, and D. Lightfoot (2008), Aboveground net primary production dynamics in a northern Chihuahuan Desert ecosystem, *Oecologia*, *155*, 123–132.

Mutziger, A. J., C. M. Burt, D. J. Howes, and R. G. Allen (2005), Comparison of measured and modified FAO 56 modeled bare soil evaporation, *J. Irrig. Drain. Eng.*, *131*, 59–72.

Myneni, R. B., C. D. Keeling, C. J. Tucker, G. Asrar, and R. R. Nemani (1997), Increased plant growth in the northern high latitudes from 1981 to 1991, *Nature*, *386*, 698–702.

Nash, J. E., and J. V. Sutcliffe (1970), River flow forecasting through conceptual models: Part 1. A discussion of principles, *J. Hydrol.*, *10*(3), 282–290.

Paul, M. N., and M. Litvak (2010), Quantifying biome specific relationships of vegetation indices and monsoon event responses, paper presented at 2009 REU Summer Symposium. [Available at http://sev.lternet.edu/documents/reu/past_projects/2009/MaxinePaul.ppt.].

Pockman, W. T., and J. S. Sperry, (1997), Freezing-induced xylem cavitation and the northern limit of Larrea tridentata, *Oecologia*, *109*, 19–27.

Porporato, A., F. Laio, L. Ridolfi, and I. Rodriguez-Iturbe (2001), Plants in watercontrolled ecosystems: Active role in hydrological processes and response to water stress. III. Vegetation water stress, *Adv. Water. Resour.*, *24*, 725–744.

Porporato, A., P. D'Odorico, F. Laio, and I. Rodriguez-Iturbe (2003), Hydrologic controls on soil carbon and nitrogen cycles. I. Modeling scheme. *Adv. Water Resour.*, *26*, 45–58.

Reid, K. D., B. P. Wilcox, D. D. Breshears, and L. MacDonald (1999), Runoff and erosion in a piñon-juniper woodland: Influence of vegetation patches, *Soil Sci. Soc. Am. J.*, *63*, 1869–1879.

Ricard, J. P., and C. Messier (1996), Abundance, growth, and allometry of red raspberry (Rubus idaeus L.) along a natural light gradient in a northern hardwood forest, *For. Ecol. Manage.*, *81*, 153–160.

Rietkerk, M., S. C. Dekker, M. J. Wassen, A. W. M. Verkroost, and M. F. P. Bierkens (2004), A putative mechanism for bog patterning, *Am. Nat.*, *163*(5), 699–708.

Rizvi, S. J. H., and V. Rizvi (Eds.) (1992), *Allelopathy: Basic and Applied Aspects*, 480 pp., Chapman & Hall, London.

Rodriguez-Iturbe, I. (2000), Ecohydrology: A hydrologic perspective of climate-soil-vegetation dynamics, *Water Resour. Res.*, *36*(1), 3–9.

Rodriguez-Iturbe, I., P. D'Odorico, A. Porporato, and L. Ridolfi, (1999), On the spatial and temporal links between vegetation, climate, and soil moisture, *Water Resour. Res.*, *35*(12), 3709–3722.

Rutherford, M. C., and M. D. Panagos (1982), Seasonal woody plant growth in Burkea africana-Ochna pulchra savanna. *S. Afr. J. Bot.*, *1*, 104–116.

Ryan, M. G. (1991), The effects of climate change on plant respiration, *Ecol. Appl.*, *1*(2), 157–167.

Sankaran, M., J. Ratnam, and N. P. Hanan (2004), Tree-grass coexistence in savannas revisited–Insights from an examination of assumptions and mechanisms invoked in existing models, *Ecol. Lett.*, *7*, 480–490.

Scanlon, T. M., K. K. Caylor, S. A. Levin, and I. Rodriguez-Iturbe (2007), Positive feedbacks promote power-law clustering of Kalahari vegetation, *Nature*, *449*(7159), 209–212.

Scholes, R. J., and S. R. Archer (1997), Tree-grass interactions in savannas, *Annu. Rev. Ecol. Syst.*, *28*, 517–544.

Schott, M. R., and R. D. Pieper (1986), Succession in pinyon-juniper vegetation in New Mexico, *Rangelands*, *8*(3), 126–128.

Scott, R. L., T. A. Huxman, W. L. Cable, and W. E. Emmerich (2006), Partitioning of evapotranspiration and its relation to carbon dioxide exchange in a Chihuahuan Desert shrubland, *Hydrol. Process.*, *20*, 3227–3243.

Seager, R., et al. (2007), Model projections on an imminent transition to a more arid climate in southwestern North America, *Science*, *316*, 1181–1184.

Shuttleworth, W. J. (1992), Evaporation, in *Handbook of Hydrology*, edited by D. R. Maidment, pp. 4.1–4.53, McGraw-Hill, New York.

Sitch, S., et al. (2003), Evaluation of ecosystem dynamics, plant geography and terrestrial carbon cycling in the LPJ dynamic global vegetation model, *Global Change Biol.*, *9*, 161–185.

Small, E. E. (2005), Climate controls on diffuse groundwater recharge in semiarid environments of the southwest United States, *Water Resour. Res.*, *41*, W04012, doi:10.1029/2004WR003193.

Soil Survey Staff (1994), *State Soil Geographic Database (STATSGO) data users guide*, USDA Nat. Resour. Conserv. Serv. Misc. Publ. 1492, pp. 88–1036, U.S. Gov. Print. Off., Washington, D. C.

Svoray, T., and A. Karnieli (2010), Rainfall, topography and primary production relationships in a semiarid ecosystem. *Ecohydrology*, *4*, 56–66.

Tilman, D. (1987), Secondary succession and the pattern of plant dominance along experimental nitrogen gradients, *Ecol. Monogr.*, *57*, 189–214.

Tilman, D. (1994), Competition and biodiversity in spatially structured habitats, *Ecology*, *75*, 2–16.

Turnbull, L., J. Wainwright, and R. E. Brazier (2010), Hydrology, erosion and nutrient transfers over a transition from semi-arid grassland to shrubland in the South-Western USA: A modelling assessment, *J. Hydrol.*, *388*, 258–272.

Van Auken, O. W. (2009), Causes and consequences of woody plant encroachment into western North American grasslands, *J. Environ. Manage.*, *90*, 2931–2942, doi:10.1016/j.jenvman.2009.04.023.

van Wijk, M. T., and I. Rodriguez-Iturbe (2002), Tree-grass competition in space and time: Insights from a simple cellular automata model based on ecohydrological dynamics, *Water Resour. Res.*, *38*(9), 1179, doi:10.1029/2001WR000768.

Vivoni, E. R., C. A. Aragon, L. Malczynski, and V. C. Tidwell (2009), Semiarid watershed response in central New Mexico and its sensitivity to climate variability and change, *Hydrol. Earth Syst. Sci.*, *9*, 715–733.

Walker, B. H., and I. Noy-Meir (1982), Aspects of stability and resilience of savanna ecosystems, in *Ecology of Tropical Savannas*, edited by B. J. Walker and B. H. Huntley, pp. 556–590, Springer, Berlin.

Walker, B. H., C. Holling, and R. M. Peterman (1981), Stability of semiarid savanna grazing systems, *J. Ecol.*, *69*(2), 473–498.

Walter, H. (1971), *Ecology of Tropical and Subtropical Vegetation*, Oliver and Boyd, White Plains, N. Y.

Wang, G. (2005), Agricultural drought in a future climate results from 15 global climate models participating in the IPCC 4th assessment, *Clim. Dynam. 25*, 739–753.

Watkinson, A. (1992), Plant senescence, *Trends Ecol. Evol.*, *7*, 417–420.

Went, F. W. (1955), The ecology of desert plants, *Sci. Am.*, *192*, 68–75.

Williams, C. A., and J. D. Albertson (2004), Soil moisture controls on canopy-scale water and carbon fluxes in an African savanna, *Water Resour. Res.*, *40*, W09302, doi:10.1029/2004WR003208.

Williams, C. A., and J. D. Albertson (2005), Contrasting short- and long-timescales effects of vegetation dynamics on water and carbon fluxes in water-limited ecosystems, *Water Resour. Res.*, *41*, W06005, doi:10.1029/2004WR003750.

Wooten, J. (2001), Local interactions predict large-scale pattern in empirically derived cellular automata, *Nature*, *413*, 841–844.

Yan, H.-P., M. Z. Kang, P. de Reffye, and M. Dingkuhn (2004), A dynamic, architectural plant model simulating resource-dependent growth, *Ann. Bot.*, *93*, 591–602.

Zeng, X. D., X. Zeng, and M. Barlage (2008), Growing temperate shrubs over arid and semiarid regions in the community land model–dynamic global vegetation model, *Global Biogeochem. Cycles*, *22*, GB3003, doi:10.1029/2007GB003014.